Bachelor Project

Czech Technical University in Prague

F3

Faculty of Electrical Engineering
Department of Cybernetics

Prediction of a Rainfall Intensity from Signal Attenuation of a Microwave Link Network

Jan Klivan

Supervisor: Prof. Dr. Ing. Jan Kybic
May 2024

BACHELOR‘S THESIS ASSIGNMENT

I. Personal and study details

Student's name: **Klivan Jan** Personal ID number: **507661**

Faculty / Institute: **Faculty of Electrical Engineering**

Department / Institute: **Department of Cybernetics**

Study program: **Cybernetics and Robotics**

II. Bachelor’s thesis details

Bachelor’s thesis title in English:

Prediction of a Rainfall Intensity from Signal Attenuation of a Microwave Link Network

Bachelor’s thesis title in Czech:

Predikce intenzity deště z útlumového signálu sítě mikrovlnných spojů

Guidelines:

Real-time measurement of rain intensity is important for meteorology, water management and for early warning against floods. However, the current monitoring network of rain gauges is not sufficiently dense. Fortunately, it is possible to estimate the rainfall intensity from the attenuation of microwave links, which are abundant in populated areas. The project goals are to select a suitable method for rain detection from the measured signals, to obtain a dense prediction of the rainfall intensity over the area of interest from all available microwave links and to test the use of a weather radar as a reference,

Procedure:

1. Familiarize yourself with the available data (radar images, information from microwave links) and existing methods.
2. Experimentally compare at least three different advanced methods for precipitation detection from attenuation signals on synthetic and real data. Evaluate the effect of the length of the time window.
3. Obtain rain/no rain information from radar imagery and compare it with rainfall gauge information.
4. Obtain an estimate of rainfall intensity from each link.
5. Detect and remove unreliable measurements based on the comparison of nearby joints. Evaluate experimentally.
6. Interpolate an estimate of the rainfall intensity in space based on all available links. Visualize the results.
7. Quantitatively and qualitatively compare the resulting estimate with measurements from rain gauges and radar data.

Bibliography / sources:

[1] M. Fencl, P. Valtr, M. Kvičera and V. Bareš, "Quantifying Wet Antenna Attenuation in 38-GHz Commercial Microwave Links of Cellular Backhaul," in IEEE Geoscience and Remote Sensing Letters, vol. 16, no. 4, pp. 514-518, April 2019, doi: 10.1109/LGRS.2018.2876696.
[2] Fencl, M., Dohnal, M., Rieckermann, J., and Bareš, V.: Gauge-adjusted rainfall estimates from commercial microwave links, Hydrol. Earth Syst. Sci., 21, 617–634, https://doi.org/10.5194/hess-21-617-2017, 2017.
[3] H. V. Habi and H. Messer, "Recurrent Neural Network for Rain Estimation Using Commercial Microwave Links," in IEEE Transactions on Geoscience and Remote Sensing, vol. 59, no. 5, pp. 3672-3681, May 2021, doi: 10.1109/TGRS.2020.3010305.
[4] Chwala, C., Keis, F., and Kunstmann, H.: Real-time data acquisition of commercial microwave link networks for hydrometeorological applications, Atmos. Meas. Tech., 9, 991–999, https://doi.org/10.5194/amt-9-991-2016, 2016.

© ČVUT v Praze, Design: ČVUT v Praze, VIC

Name and workplace of bachelor's thesis supervisor:

prof. Dr. Ing. Jan Kybic Biomedical imaging algorithms FEE

Name and workplace of second bachelor's thesis supervisor or consultant:

Date of bachelor's thesis assignment: **01.02.2024** Deadline for bachelor thesis submission: **24.05.2024**

Assignment valid until: **21.09.2025**

prof. Dr. Ing. Jan Kybic Supervisor's signature	prof. Dr. Ing. Jan Kybic Head of department's signature	prof. Mgr. Petr Páta, Ph.D. Dean's signature

III. Assignment receipt

The student acknowledges that the bachelor's thesis is an individual work. The student must produce his thesis without the assistance of others, with the exception of provided consultations. Within the bachelor's thesis, the author must state the names of consultants and include a list of references.

.	
Date of assignment receipt	Student's signature

© ČVUT v Praze, Design: ČVUT v Praze, VIC

Acknowledgements

I would like to thank prof. Dr. Ing. Jan Kybic for his support, insights, and expert guidance. Also, I would like to thank Ing. Vojtěch Bareš, Ph.D. and Ing. Anna Špačková for their consultations, ideas, and data that I used in this work. Lastly, I would like to thank my family for their support.

Declaration

I declare that the presented work was developed independently and that I have listed all sources of information used within it in accordance with the methodical instructions for observing the ethical principles in the preparation of university theses.

Prague, May 24, 2024

Abstract

Rainfall estimation from commercial microwave links is a method whose potential use is to supplement the estimates of the existing rain gauge network or to be used in case of its absence. This method is the subject of scientific research, and many approaches have been developed, some of them are based on physics models and others on neural networks. In this work, we focus on testing several new methods for the task of wet/dry classification and for the task of rainfall intensity estimation. First, we test individual methods on the selected group of links and then extend the best-performing method for use on all links. Furthermore, we investigate the usage of weather radar snapshots instead of rain gauges as reference, because weather radars cover a larger area than rain gauges. We concluded that for the task of wet/dry classification neural network of P. Novota is better, however for the rainfall estimation task from all links our recurrent network inspired by Habi et al. obtains better results.

Keywords: rain intensity estimation, commercial microwave links, neural networks, weather radar

Supervisor: Prof. Dr. Ing. Jan Kybic

Abstrakt

Odhad množství spadlého deště z komerečních mikrovlnných je metodou jejíž potenciální využití je pro doplnění odhadů stávající srážkoměrové sítě či využití v případě její absence. Metoda je předmětem vědeckého zkomumání a byla vyvinutá celá řada přístupů některé z nich jsou založeny na fyzikálních modelech jiné na neuronových sítích. V této práci se zabýváme otestováním několika nových metod pro úlohy klasifikace do tříd prší/neprší a pro úlohu odhadu srážkové intenzity. Prvně testujeme jednotlivé metody na vybrané skupině spojů a následně nejlepší metodu rozšíříme pro použití na všech spojích. Dále zkoumáme možnost využití radarových snímku z meteorologického radaru namísto srážkoměrů jako referečnídat, protože meteorologické radary pokrývají větší území než srážkoměry. Naším závěrem je, že zatímco pro klasifikaci prší/neprší funguje lépe neuronová síť P. Novoty, tak pro odhad srážkové intenzity ze všech spojů funguje lépe námi představená rekurentní síť inspirovaná Habi et al.

Klíčová slova: odhad srážkové intenzity, komereční mikrovlnné spoje, neuronové sítě, meteorologický radar

Překlad názvu: Predikce intenzity deště z útlumového signálu sítě mikrovlnných spojů

Contents

1 Introduction **1**
1.1 Existing methods 2
1.1.1 Wet-dry classification 2
1.1.2 Model-based rain estimation . . 2
1.1.3 Data-driven methods 4
1.2 Standard methods of a rainfall measurement 4
1.2.1 Rain Gauge 4
1.2.2 Weather Radar 4

2 Methods **7**
2.1 Dataset 7
2.2 Preprocessing 10
2.2.1 Microwave links 10
2.2.2 Weather radar 11
2.3 Input data preprocessing 13
2.4 Wet-dry classification 13
2.4.1 Residual network model 14
2.4.2 Recurrent model 15
2.4.3 Training and loss function . . . 16
2.5 Rainfall estimation 16
2.5.1 Residual network model 16
2.5.2 Recurrent model 17
2.5.3 Multi-link model 17
2.5.4 Antenna attenuation model . 18
2.5.5 Training and loss function . . . 18
2.5.6 Interpolation 19

3 Experimental results **21**
3.1 Evaluation metrics 22
3.1.1 Classification 22
3.1.2 Regression 22
3.2 Weather radar comparison with rain gauges 23
3.2.1 Spacial correlation of weather radar with rain gauges 25
3.3 Wet-dry classification 26
3.4 Rainfall estimation 31
3.5 Multi-link rain estimation 35
3.5.1 Link-based comparison 35
3.5.2 Map-based comparison 38

4 Discussion **41**

5 Conclusion **43**

Bibliography **45**

A Interpolation maps **49**

Figures

2.1 Examples of the link attenuation signal 7
2.2 Example of a radar snapshot 8
2.3 Distribution of CMLs (gray lines) and rain gauges (blue crosses) in Prague 8
2.4 Step histogram for one of the "multi" datasets 9
2.5 Simulated data for the link 56 . . 10
2.6 Signal attenuation before aggregation 11
2.7 Signal attenuation after aggregation 11
2.8 Reflectivity scale of radar snapshot 12
2.9 Local rain event over link 56 on 23.05.2015 12
2.10 Computed rain intensity along the path of the link 56 13
2.11 Residual network architecture with tensor shapes between each layer in order channels, time 14
2.12 Residual block, part marked with dotted line is included only if the input and the output of the residual block have a different number of channels, otherwise the shortcut connection is without convolution . 15
2.13 Recurrent network architecture with tensor shapes between layers in order channels, time 15
2.14 MSE error on the test set during training with the original network (blue) and our modified version (orange). 16
2.15 Recurrent multi link model with tensor shapes in order channels, time. Static data represents information about the link as additional to the input 17
2.16 Antenna attenuation model with tensor size in order channels, time 18
3.1 Comparison of weather radar with the rain gauges for time intervals from 1 hour to 24 hours. The blue dashed line is an ideal relationship between measured rainfalls and the red dashed line is a linear fit using the least squares method 23
3.2 Comparison of weather radar with the rain gauges for different seasons with one hour aggregation 24
3.3 Comparison of the RG1 and RG10 rain gauges with the radar reference with one hour aggregation 24
3.4 Wet-dry classification from weather radar using rain gauges as a reference with time aggregation of 15 minutes and without spatial aggregation. Flat parts of the graph are caused by the logarithmic scale of the radar. 25
3.5 Effect of time and spacial aggregation on NRMSE error between the rain gauges and weather radar 25
3.6 MCC score comparison 27
3.7 Confusion matrices for different methods for the link 444. All methods have hyperparameters set to maximize MCC score on the part of the train set as was described in the beginning of this section 27
3.8 Confusion matrices for different methods for the link 444 28
3.9 Recall score for different minimal rain intensities for link 444 28
3.10 Recall score for different minimal rain intensities for the link 253 . . . 28
3.11 ROC and Precision-Recall curves for link 253 29
3.12 Examples of the wet-dry classification for link 253, green is correctly classified wet period, orange is falsely detected wet period and red is missed wet period 30
3.13 Distribution of WAA coefficients for model-based estimation method 31

Tables

3.1 Selected link parameters 26
3.2 F1 score, sim are simulated data for link 444 26
3.3 RMSE values for different methods 31
3.4 RMSE values for different rain intensities for link 253 32
3.5 RMSE values for different rain intensities for the link 63 33
3.6 RMSE comparison with radar reference for different time aggregations. 37
3.7 RMSE values for different rain intensities using all CML links. . . . 37
3.8 RMSE between methods and radar maps with different time aggregations 38
3.14 Rain intensity estimation on link 444 for different methods 32
3.15 NRMSE of selected methods for different rain intensities for link 253 33
3.16 NRMSE of selected methods for different rain intensities for the link 63 33
3.17 Static baseline method 34
3.18 Recurrent network 34
3.19 Comparison of CML estimated rainfall with radar reference for one hour aggregation. 35
3.20 Comparison of CML estimated rainfall with radar reference for two hour aggregation. 36
3.21 Comparison of CML estimated rainfall with radar reference for twelve hour aggregation 36
3.22 Comparison of CML estimated rainfall with radar reference for 24 hour aggregation. 36
3.23 Spikes in attenuation of the link 69 37

A.1 Example of the interpolation maps for the different methods for the low rain intensity on 2015-08-16 14:00 . 50
A.2 Example of the interpolation maps for the different methods for the middle rain intensity on 2015-09-06 02:00 51
A.3 Example of the interpolation maps for the different methods for the high rain intensity on 2015-09-07 12:30 . 52

May 24, 2024

Chapter 1

Introduction

Commercial microwave links (CMLs) are primarily used for the transfer of information and are often used by telephone companies. Many of them operate on frequencies between 20 and 40 GHz. The relationship between the rain intensity and the rain-induced attenuation is complex[1], and it depends on the distribution of droplet sizes which is often unknown. However, in this particular range, there is almost a linear relationship between the link attenuation and the rain intensity, therefore a simplified equation can be derived. CMLs can be potentially used as rain gauges, this data can be useful for example for creating more precise rainfall maps in areas with a smaller number of rain gauges, but with a larger number of CMLs, which is often the case in developing countries.

Experiments with estimation of a rainfall intensity from microwave signal attenuation date back to 1942[1], when the first pioneering experiments were performed in Hawaii. But recently it has become a topic of interest because of the extensive growth of cellular networks, which usually contain many CMLs as part of their infrastructure.

Messer et al. [2] firstly proposed the usage of existing commercial microwave links for rainfall estimation, where they had shown on one selected CML in Tel-Aviv and Haifa correlation between its signal attenuation and rain gauge reference. Since then, with the rising number of CMLs, the amount of available data has grown. Processing of data can be divided into two main categories one where the model is based on physics theory (model-based) and one where the model is estimated from data (data-driven).

Model-based processing is based on modeling the rain-induced attenuation, although the relation itself is complex it can be simplified for certain frequencies.

On the other hand data-driven processing, which often uses deep learning, usually does not require any predefined models and tries to use patterns from data to learn the model that matches the input data. In this work, we also will focus on the deep learning approach to data-driven processing and compare it with the model-based ones.

The second goal of this work is to investigate the usage of data from weather radar as a reference for the rain estimation based on CMLs signal attenuation

and to obtain rain estimation from all available links.

1.1 Existing methods

1.1.1 Wet-dry classification

Wet-dry classification classifies periods with fixed length as wet when their mean rain intensity is above a certain threshold. One way to approach this is with simple thresholding when above a certain threshold σ of the mean link attenuation A_n in the period n we will say that period is wet.

$$\hat{C}_n = \begin{cases} 1 & A_n > \sigma \\ 0 & \text{otherwise} \end{cases} \tag{1.1}$$

$\hat{C}_n$ is an estimated wet-dry classification where 1 means wet period and 0 dry period. This method is not widely used, because it does not work when baseline attenuation of the link, which is not induced by the rain, changes over time.

Another classification method uses rolling standard deviation of the CML attenuation.

$$\sigma_n = \sqrt{\frac{1}{N} \sum_{k \in W_n} \left(A_k - \overline{A_k}\right)^2} \tag{1.2}$$

W_n is a moving window in the range $[n - N, n]$, N is window size and A_k is attenuation sample from the moving window. The moving window contains samples of the link attenuation A. Windows can but do not need to overlap. Classification is then performed based on the threshold σ_t.

$$\hat{C}_n = \begin{cases} 1 & \sigma_n > \sigma_t \\ 0 & \text{otherwise} \end{cases} \tag{1.3}$$

The above methods work only with one link at a time. A. Overeem et al. [3] used multiple links for better wet-dry classification, based on the assumption that in case of a rain event, more than half of the links in a certain radius around the selected link must experience a similar increase in signal attenuation. This method however also requires sufficient density of CMLs network to work.

1.1.2 Model-based rain estimation

Attenuation of a microwave link consists of three main terms and can be modeled as

$$A(t) = A_r(t) + A_b(t) + A_a(t) \tag{1.4}$$

A_r is rain-induced attenuation, A_b is baseline attenuation, A_a is wet antenna attenuation, and terms A_b and A_r also depend on frequency, length, and polarization of the link.

A_r is complex and depends on droplet size, but for frequencies around 30 GHz it can be simplified as

$$A_r(t) = \alpha R(t)^\beta \tag{1.5}$$

R is the rain rate and α, β are constants that depend on the link length, frequency, and polarization. Coefficient β is approximated as $\beta \approx 1$ for frequencies around 30 GHz [4] and coefficient α is expressed as aL where L is link length. To relation (1.5) is often referred to as the k-R relation.

A_b is baseline attenuation which is mainly caused by an air permittivity, and it is relatively easy to estimate because it mostly depends on path length, however it also changes over time (but slower than the rain attenuation), because of differences in signal scattering due to changing atmospheric conditions.

Baseline attenuation can be estimated using wet-dry classification because it changes largely during dry periods. Using wet-dry classification $\hat{C}$, A_b is than estimated as

$$\hat{A}_n^b = \begin{cases} A_n & \hat{C}_n = 0 \\ A_{n-1}^b & \hat{C}_n = 1 \end{cases} \tag{1.6}$$

To this method, we will refer as a static baseline method, because it assumes that the baseline is static during the wet period.

Another approach is estimation of baseline attenuation dynamically as a function from a set of consecutive samples.

$$\hat{A}_n^b = f\left(A_n, A_{n-1}, \cdots, A_{n-N}\right) \tag{1.7}$$

Where N is the size of the input to the function f. This function is often selected as *min*, other options are *median* or *quantile* functions. We will refer to this method as a dynamic baseline.

Last term A_a is wet antenna attenuation. Wet antenna attenuation is specific for each CML, it is caused by absorption of humidity by the antenna cover. Because A_a is complex and hard to predict multiple models tries to model it [5], [6], [7]. In this work we will use model proposed by J. Pastorek et al. [6], because its performance was evaluated in their paper on part of our dataset and showed the best results together with the model from [7]. It is modeled as

$$A_a(R) = C\left(1 - \exp\left(-dR^z\right)\right) \tag{1.8}$$

C,d,z are constant coefficients of the model, computed for each link. This model depends on the rain intensity, which is however unknown during the computation of A_a, in their paper they first computed the rain rate from raw data with baseline subtracted but without WAA correction, then

they subtracted computed WAA, and did this process again. We will use the version implemented in Pycomlink library[1], where instead of doing an iterative process every time a lookup table is built for different values of attenuation, to speed up the computation.

This method is used in many works for example in Gemany[8], Czech Republic[9], Africa [10] or Brazil[11]. The main difference between each use case is in the baseline and WAA estimation.

1.1.3 Data-driven methods

In the case of data-driven methods, the rain intensity and the wet-dry classification are estimated by the neural network directly from the input link attenuation. One approach to this problem is the usage of convolutional networks. convolutional networks are widely used for classification task in image and signal processing and were successfully used on CMLs data in Germany[12] and in the Czech Republic[13]. Each architecture differs, in[12] they used a plain feed-forward convolutional network whereas in [13] convolutional network with skip connections was used instead. In [12] the evaluated dataset was also larger with 3904 CML links compared to 28 in [13].

A different approach is the usage of recurrent networks, which can learn time-dependent patterns in data. Recurrent networks are used in speech recognition, signal classification, and regression tasks. Their performance was tested in [14] on datasets from Izrael and Sweden, and showed very good results compared to the model-based method of rainfall estimation.

1.2 Standard methods of a rainfall measurement

1.2.1 Rain Gauge

Rain gauges are devices that measure the amount of rainfall, a common type of rain gauge is one with a tipping bucket, which is why they are often referred to as tipping bucket rain gauges. When one half of the tipping bucket fills with a predefined amount of water it tips and the other half fills. With every tipping predefined amount of rainfall is measured. Advantages are reliability and accuracy, however accuracy is limited by the size of tipping the bucket with a bigger gauge that may not catch the beginning of light rain [15]. A disadvantage especially for hydrological monitoring is the spatial density.

1.2.2 Weather Radar

Weather radar measures the amount of water accumulated in clouds using the reflectivity of water droplets. The relation between the reflectivity and the rain rate is complex and depends on many factors but as in the case of

[1] Pycomlink - `https://pycomlink.readthedocs.io/en/latest/`

the rain attenuation, it can be simplified using power law as

$$Z = \alpha R^{\beta} \tag{1.9}$$

Z is signal reflectivity, R is rain intensity and α, β coefficients depend on the specific types of precipitation (hails, snow, rain). This relation is often referred to as Z-R relation. Reflectivity is usually expressed in dBZ (decibel relative to Z).

Weather radar has better spatial density than rain gauges because one radar antenna covers a bigger area. However, a disadvantage of the radar is that it measures the amount of water in clouds not the actual amount dropped from them, other factor is that clouds' base is for the lowest clouds around $1 - 2$ km above ground, and when droplets fall their impact location can differ, which results in inaccuracies when taking measurements directly in locations of the radar grid [16].

Chapter 2

Methods

2.1 Dataset

For creating a dataset were available data from 422 full duplex CMLs from Prague together with 23 rain gauges. We also have a weather radar reference in the form of PNG pictures. In the figure 2.3, we can see the distribution of the rain gauges and CMLs around Prague. The length of each CML spans from 48 to 10257 m and frequencies from 18 to 39 GHz. The sampling frequency of each link ranges from 0.5s to 15s, with quantization of 1dB and 0.33 dB. The time range of the CML dataset is from 2014 to 2017, although not every link has the same time span.

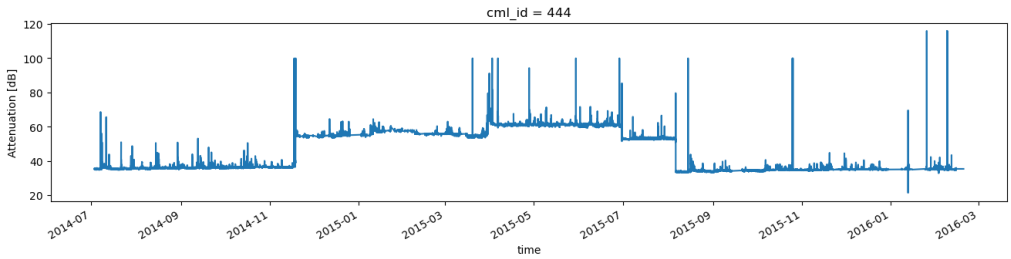

(a) : Link 444

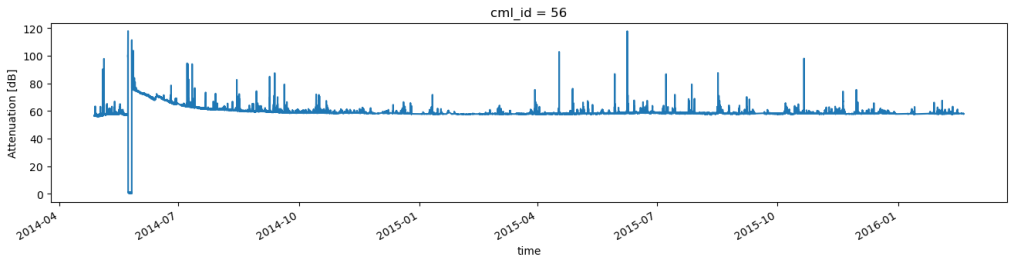

(b) : Link 56

Figure 2.1: Examples of the link attenuation signal

Weather radar data consist of PNG snapshots for the whole Czech Republic captured in 15-minute intervals with resolution around 1 km^2 per pixel. Time

span is from 2014 to 2016 and only a few snapshots in this time range are missing. These PNG snapshots are from the Czech Hydrometeorological Institute and information about their weather radars can be found at [17](only in Czech).

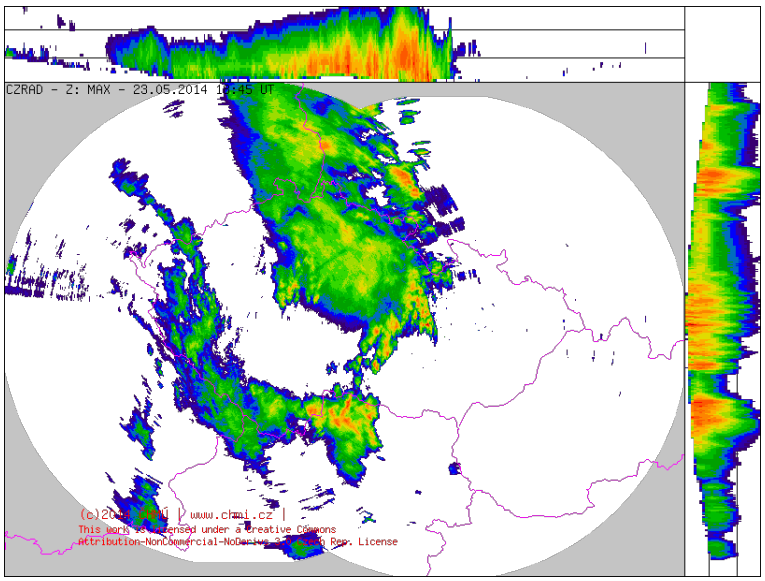

Figure 2.2: Example of a radar snapshot

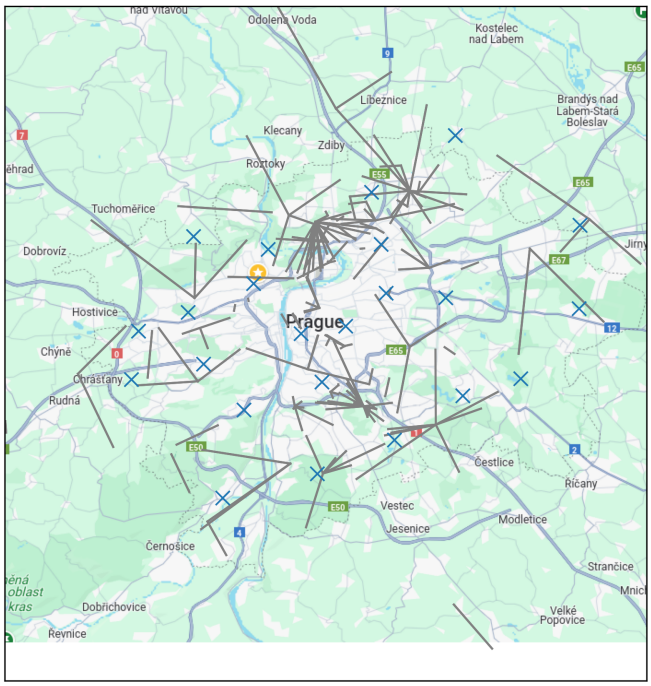

Figure 2.3: Distribution of CMLs (gray lines) and rain gauges (blue crosses) in Prague

For the rain gauges, we have data from 23 tipping bucket rain gauges. Data time ranges from 2014 to 2017. The sampling rate is one minute and measurements are recorded as rain intensities in mm/h. The resolution of the data is 0.4 mm/h.

Temperature data that were used for filtration of the solid-state precipitation were available from meteorological station Prosek with a sampling rate of one minute.

All data can be found in "/datagrid/Medical/tel4rain_radar" folder on computers of the Department of Cybernetics.

To train the neural network, two different types of datasets were created. Datasets for each link and datasets containing all links. Because the time range of the weather radar combined with CMLs is limited to only a year and a half of data (most of the links range from 2014-07 to 2016-03) and we wanted to divide data into continuous sections, to eliminate the correlation between them, we divided data only to the train and test set. For the individual links, we selected the period from 2014 to 2015-07 as the train set and from 2015-08 to 2015-12 as the test set. We will call this type of datasets "individual".

For training with multiple links we created five datasets for the cross-validation where test data are divided in time same as on individual links, but furthermore, test links are not included in the train set, this minimizes not only time correlation but also space correlation between the train and test set. We will call this type of dataset "multi".

Step histograms for one of the "multi" datasets are in the figure 2.4 with the step of 2 mm/h without overlapping of each bin.

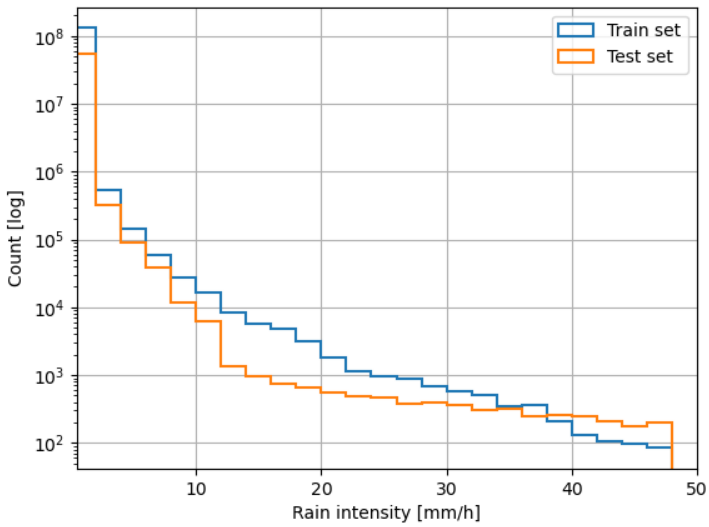

Figure 2.4: Step histogram for one of the "multi" datasets

We also created a synthetic data generator. It takes rain reference as the input and models the output attenuation. This is done by firstly using the k-R

relation (1.5) to generate rain attenuation, then adding noise only to the rain events together with WAA (we used the model from [6]). In the last step, we added slowly changing baseline and random noise, which was generated using Cauchy distribution. Cauchy distribution was selected because it simulates spikes in the signal attenuation which often occurr in real CMLs data. An example of simulated data for the link 56 is shown in the figure 2.5.

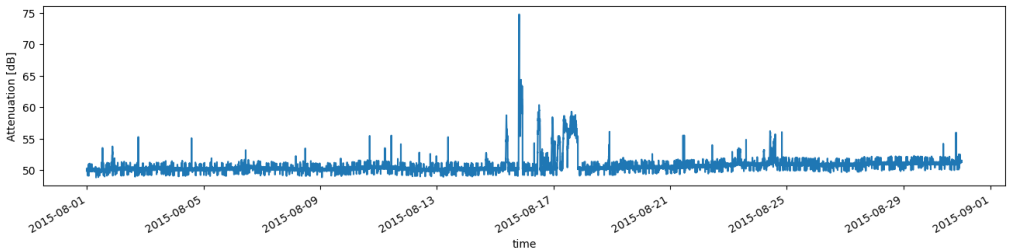

(a) : Simulated attenuation

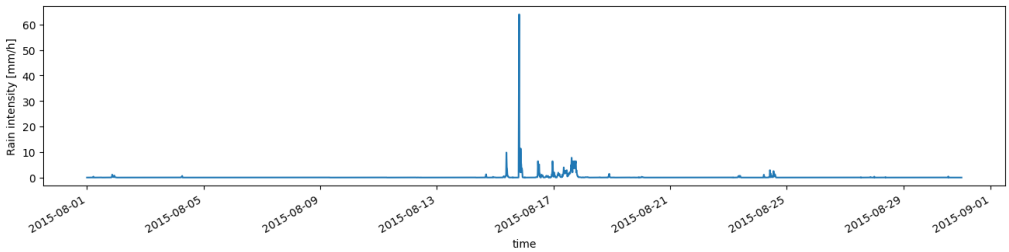

(b) : Reference rain intensity from the radar

Figure 2.5: Simulated data for the link 56

2.2 Preprocessing

2.2.1 Microwave links

For every CML is available received and transmitted power with a timestamp. Each CML differs in its length, polarization, and frequency. Many of the links have automatic regulation of the transmitted power so that the received power on the other side stays constant, this automatic regulation differs between the links, which is why we will work with the difference between transmitted and received power, which suppresses the effect of the automatic regulation.

$$A(t) = P_{tx}(t) - P_{rx}(t) \tag{2.1}$$

A is measured attenuation, P_{tx} is transmitted and P_{rx} received power.

The first step in CML preprocessing is to unite sampling intervals across CMLs. We choose 1 min as the sampling interval, with *mean* as the aggregate function, because the sampling frequency of CMLs is less than one minute. One minute provides high enough time resolution, but also partially suppresses the noise as can be seen in the figure 2.7.

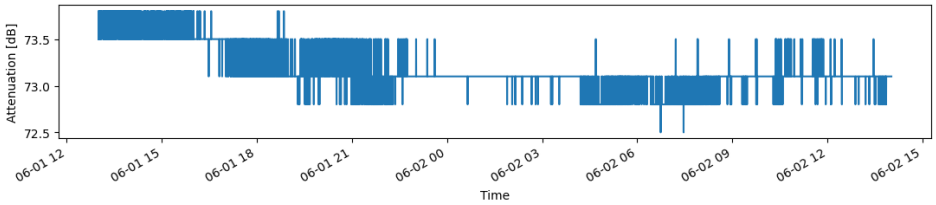

Figure 2.6: Signal attenuation before aggregation

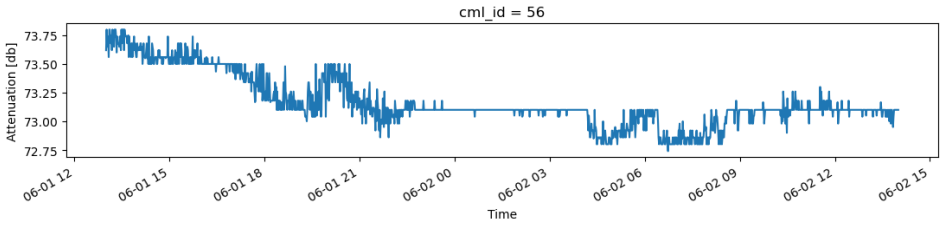

Figure 2.7: Signal attenuation after aggregation

The next step is a removal of the outliers where the attenuation values are $A_{min} = -99$ or $A_{max} = 255$ and of the measurements during which the air temperature was below $4°C$ because the relation(1.5) for the rain attenuation applies well only for liquid precipitation [6]. Removed data are replaced for smaller ranges (under 5 min) with an interpolation.

2.2.2 Weather radar

The representation of colors in the PNG snapshot files is not in RGB format but in a color palette, where every color is encoded as one 8-bit number. The color palette represents rain intensity and reflectivity at the same time. The scale of the reflectivity is linear, and it ranges from 4 dBZ to 60 dBZ, whereas the scale of the rain intensity is logarithmic (decadic logarithm), and it ranges from 0.01 mm/h to 331 mm/h.

The color palette in the range from 181 to 195 is mapped to the rain intensities using equations (2.2) and (2.3), outside this range are colors that are used to display country borders for a text and other graphical components see figure 2.2.

$$Z = \alpha C + \beta \tag{2.2}$$

$$R = \left(\frac{10^{Z/10}}{200}\right)^{\frac{5}{8}} \tag{2.3}$$

C is a number encoding color, R is rain intensity in mm/h, Z is reflectivity in dBZ, coefficients α, β are $\alpha = -4, \beta = 784$ and equation (2.3) is Marshall-Palmer formula[18] to compute the rain intensity from the reflectivity.

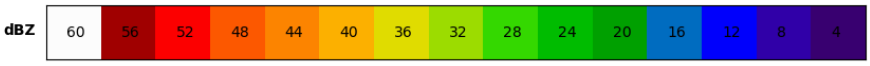

Figure 2.8: Reflectivity scale of radar snapshot

The color range of rain intensities is visualized in the figure 2.8. The next step was to map radar snapshots onto geographic coordinates using a gnomonic projection implemented in PyProj library[1]. Parameters for the gnomonic projection where consulted with Ing. Vojtěch Bareš, Ph.D. from the faculty of Civil Engineering CTU.

The last step was the computation of the weighted average of the rain intensities along each CML path

$$I_p = \sum_{i=0}^{N} w_i I_i \tag{2.4}$$

$$w_i = \frac{L_{int}}{L_p} \tag{2.5}$$

I_p is weighted rain intensity over path p, w_i and I_i are weights and rain intensities corresponding to each intersected pixel of the radar grid.

Each weight is computed as the fraction of the intersected length L_{int} and the whole link length L. Intersected length is usually computed numerically, in our case the whole computation is done by Pycomlink library[2].

After computation of the weighted average, resulting data are resampled to the time resolution of one minute, so they have the same sampling rate as the CMLs attenuation data. An example of a local rain event and the computed rain intensity along the selected CML path can be seen in figures 2.9,2.10.

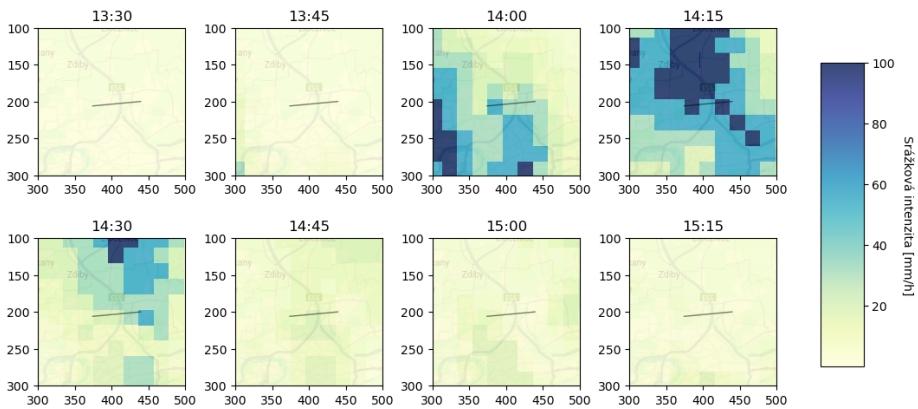

Figure 2.9: Local rain event over link 56 on 23.05.2015

[1]PyProj - https://pyproj4.github.io/pyproj/stable/
[2]Pycomlink - https://pycomlink.readthedocs.io/en/latest/

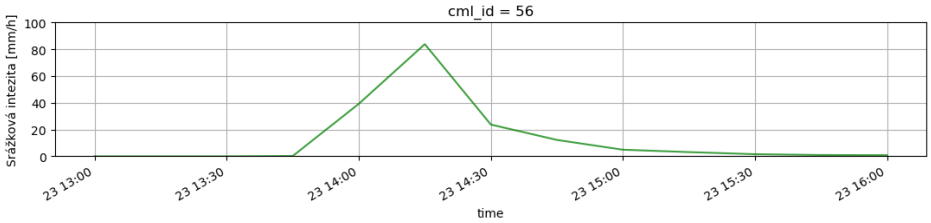

Figure 2.10: Computed rain intensity along the path of the link 56

2.3 Input data preprocessing

The input of all networks x_n is a fixed length window from the signal attenuation A in our case window size is 180 samples because it was the best trade off between network size and its performance, with longer window size, results were slightly better, however network training was much slower. The window step is one sample for the "individual" dataset to have more training steps and 32 for training with the "multi" dataset. To normalize the input data, the minimum of the values in the window is subtracted from it, without this normalization training process is slow, especially in the case of training on the "multi" dataset. Pseudocode for generating x_n and its reference r_n is shown below

Listing 2.1: Pseudocode for generating signal attenuation windows x_n and its reference windows r_n

```
input: A, R, window_size, window_step, threshold
output: x, r
begin
i ← 0
n ← 0
while i ≤ (size(A) − window_size):
    a_window ← A[i:(i + window_size)]
    x[n] ← a_window − min(a_window)

    R_window ← R[(i + window_size − window_step):(i + window_size)]
    r[n] ← R_window

    i ← i + window_step
    n ← n + 1
end
```

R is reference rain intensity for signal attenuation a, x is array of attenuation windows with corresponding reference windows r.

2.4 Wet-dry classification

In this part, we will focus on classification when it is raining and when it is not. It is a simplification of the rainfall estimation problem but still wet-dry classification is an important task for the hydrological modeling, and it is even part of the model-based method that we are using as was mentioned in the chapter 1.1. Wet-dry classification is based on the pre-set threshold for the

rain intensity above which is considered that it is raining. For the training, we chose a threshold of 1 mm/h which represents light rain. Choosing a lower value would encounter reference limitations from the weather radar, because often radar detects light precipitation in higher layers of the atmosphere which is not detected on the ground level, or it detects dust particles as precipitation [16]. We propose different network architectures for solving the wet-dry classification task each one has its advantages and disadvantages. Firstly we start with convolutional networks, which are often used in image and signal classification. However, their disadvantage is that they do not take into account time dependency between samples. For this reason, we will also propose a recurrent network architecture inspired by H. V. Habi and H. Messer [14] with different modifications.

2.4.1 Residual network model

The residual network is a well known architecture pattern used in image classification, and it shows also very good results for the signal classification [19]. It consists of multiple convolution layers stacked in blocks (residual blocks), between these layers are skip connections, which are linear shortcuts for better gradient backpropagation and thus faster network training. Our architecture can be seen in the figure 2.11 together with the detail of the residual block 2.12. It contains eight residual blocks, whose outputs are averaged with the average pool layer. The last part is the fully connected layer with the sigmoid activation function.

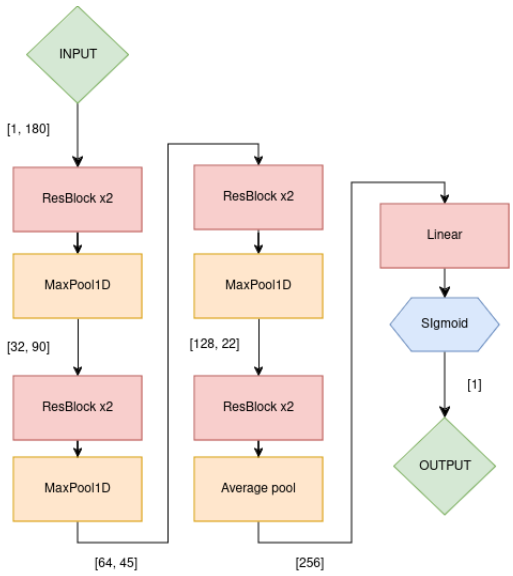

Figure 2.11: Residual network architecture with tensor shapes between each layer in order channels, time

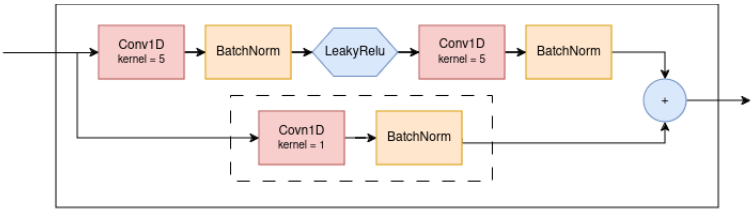

Figure 2.12: Residual block, part marked with dotted line is included only if the input and the output of the residual block have a different number of channels, otherwise the shortcut connection is without convolution

All convolution layers except for the one specified in the residual block diagram 2.12 have parameters *kernel size=5*, *stride=1* and padding so that the output size of time dimension is the same as the input one.

2.4.2 Recurrent model

The Second proposed architecture is based on the recurrent network of H. V. Habi and H. Messer [14]. Recurrent networks are widely used in speech recognition, word tagging, and signal classification thanks to their ability to learn time-dependent patterns. We modified the input of the network, in [14] where it goes directly into the GRU layer. In our modification, it firstly propagates through the convolution layer and then through the small fully connected layer over the convolution channels. This modification smooths the training of the neural network as can be seen in the figure **??** and leads to better results. Full architecture can be seen in the figure 2.13.

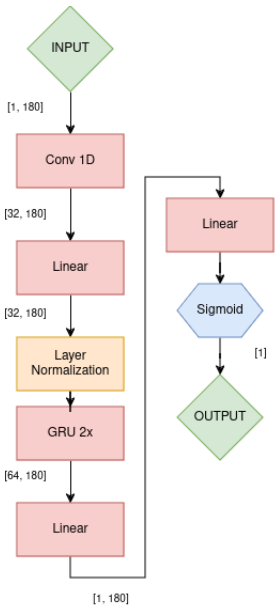

Figure 2.13: Recurrent network architecture with tensor shapes between layers in order channels, time

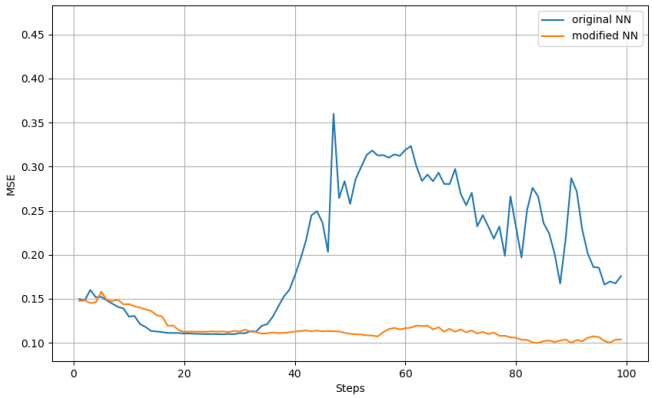

Figure 2.14: MSE error on the test set during training with the original network (blue) and our modified version (orange).

2.4.3 Training and loss function

Output y_n of the networks is a sigmoid function whose values are in the range $y_n \in [0,1]$ and based on a selected threshold we can alter between precision and recall. Classification of wet and dry periods is for the last 15 samples of each window. The loss function therefore compares the output of the sigmoid function with the thresholded mean of the last 15 samples from the reference window.

Focal loss was selected as a loss function which is a modified version of the cross entropy loss to tackle the problem of class imbalance originally developed for the object recognition task [20]. Focal loss can be written as

$$\text{Loss}(L) = -\alpha(1 - e^{-L})^{\gamma} L \tag{2.6}$$

L is binary cross entropy loss and α and γ are hyperparameters, in our case the best results were achieved with parameters $\alpha = 0.03$ and $\gamma = 2$.

2.5 Rainfall estimation

The next step is training a model for the rainfall estimation, which is our main goal. Because wet-dry classification is a simplification of the rainfall estimation we will use the modified versions of the network architectures from the wet-dry classification section.

2.5.1 Residual network model

We will use the same model as in the section 2.4.1, but with slight modifications. The first modification is the removal of the activation function after the last fully connected layer, to enable easier gradient backpropagation, the

second step is disabling bias in the whole network to prevent unwanted bias at the output.

2.5.2 Recurrent model

The architecture is almost the same as in the section 2.4.2, but we removed the activation layer function together with the last fully connected layer, which reduces the time dimension to a single point, to be able to compute output values for each input sample simultaneously. It is also possible to do this in the residual network, but that would require the removal of max pooling layers that reduce the size of the time dimension and would lead to a large growth in the network size.

Outputting the rain intensity prediction for each sample gives the network more information during backpropagation. As in the case of the residual network we disabled bias in all layers, but we also removed layer normalization, because for the regression task, we do not want to normalize data inside the network.

2.5.3 Multi-link model

Previous models could only work with one link on which they were trained. In the chapter with experimental results, we selected the best-performed network on individual links and extended it to support learning from multiple links. To be able to train the model on different links we needed to incorporate a way to use information about the link (length, frequency) in the training. We come up with the solution in the form of a small fully connected layer which takes as the input frequency and length of the link and its output is concatenated with the output of the recurrent layers see figure 2.15. We then trained this model on all available links and performed a cross validation.

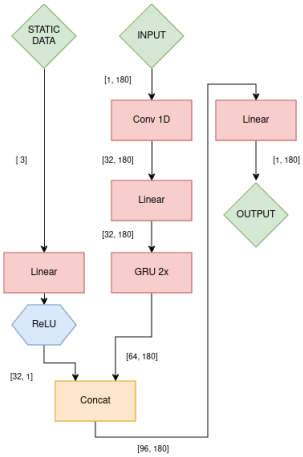

Figure 2.15: Recurrent multi link model with tensor shapes in order channels, time. Static data represents information about the link as additional to the input

2.5.4 Antenna attenuation model

For the rainfall estimation, we also created a new model. All previous models tried to compute the rain intensity directly from the signal attenuation, which is a complex task because it involves separation of the rain attenuation from the baseline A_b and the wet antenna attenuation A_a and learning relation (1.5). We tried to simplify this task by only modeling A_a and subtracting it from the input signal attenuation and then computing estimated rain intensity from the k-R relation. Because the input data are normalized by subtracting the minimum from them, it is also a type of baseline separation as we described in the chapter 1.1. The model can be seen in the figure 2.16.

Rain intensity is computed as

$$R = \left(\frac{A_r}{\alpha L}\right)^{1/\beta} \tag{2.7}$$

This equation is derived from the equation (1.5), L is the length of the link in km.

Coefficients α, β are used from the ITU-R(2005) table [21], which is part of ITU-R recommendations developed by the ITU(International Telecommunication Union). This table relates α, β to the frequency of the link.

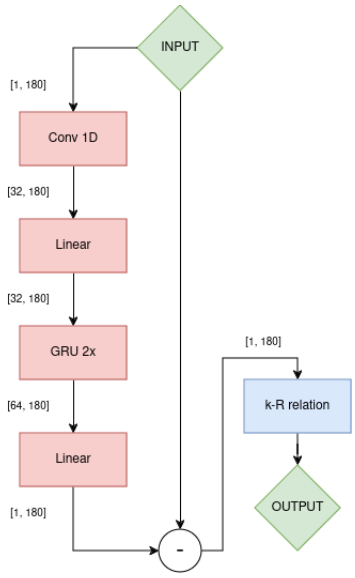

Figure 2.16: Antenna attenuation model with tensor size in order channels, time

2.5.5 Training and loss function

The input of the networks is the same as in the case of the wet-dry classification, but because the output of the models with recurrent layers can predict rain intensity for each input sample, the step of the time window can be greater than one minute. We keep one minute for the training on each link but

to speed up the training of all links we choose a step of 32 minutes. Loss function was selected MSE.

For training of the multi-link architecture we tried to filter unreliable links. One way of filtering is filtration before the training process based on suitable criteria, another option is to filter faulty links based on their loss after feed-forward of the neural network, this method is called robust learning. We used the modified loss function that filters out the worst 10% of losses each training step, therefore filtering worst performed 10% of the training links. The loss function we used is from [22], and it is defined as

$$\text{Loss}(\boldsymbol{r}) = \frac{1}{H}\sum_{i=1}^{H} r_{i:N} \tag{2.8}$$

$$r_i = \frac{1}{N}\sum_{i=0}^{N}(\hat{x}_i - x_i)^2 \tag{2.9}$$

where $r_{1:N} < \cdots < r_{N:N}$, $\hat{x}_i$ are estimated values, x_i are true values and $H < N$. In our case H is $H = 9/10N$

2.5.6 Interpolation

In the section about estimation from all available CMLs we interpolated results in space, for this task we used the inverse distance weighting method (IDW) which is computed as

$$R_p = \sum_{i=0}^{H} w_{i:N} R_i \tag{2.10}$$

$$w_i = \frac{\varphi(d_{pi})}{\sum_{x=0}^{N}\varphi(d_{px})} \tag{2.11}$$

R_p is point for which we are computing rain intensity, d_{pi} is distance between point p and i, w_i are weights satisfying $w_{1:N} > \cdots > w_{1:N}$ and $\varphi(x)$ is weight function which in case of IDW is defined as $1/x^{\alpha}$, where α is in our case two. Parameter H is a number of the closest points i to point p, that we want to consider.

Chapter 3

Experimental results

In this chapter, we will compare our results for different network architectures with other methods. We will start with a comparison of selected individual links, to find which method is most suitable for the rainfall estimation and then extend it for the training with multiple links. Five different methods for the wet-dry classification (two model-based ones and three neural networks) and six methods for the rainfall estimation (one model-based with two variations and four neural networks) will be used.

We are now going to briefly describe evaluating methods, with their shortened names in brackets that we will be using in graphs and tables. For the wet-dry classification, we will use model-based methods, one based on simple thresholding of the signal attenuation (threshold), one based on standard rolling deviation (RSD). All these methods were described in the section 1.1. For data-driven methods we will use the ResNet architecture described in the section 2.4.1 and the recurrent network (recurrent) described in the section 2.4.2 and compare them with the network proposed by P. Novota in [13] (Novota).

For the rainfall prediction, we will use the model-based rainfall estimation method described in the chapter 1.1 but with different baseline estimation methods one based on the wet-dry classification (static) and the other one based on the values of the last N samples (dynamic) both also described in the chapter 1.1. Once more we will use ResNet and the recurrent network as for the wet-dry classification but with changes as we described in the sections 2.5.1 and 2.5.2. Furthermore, we will use new a model for the estimation of WAA described in the section 2.5.4 (WAA), again we will compare these methods with the neural network by P. Novota.

3.1 Evaluation metrics

To evaluate methods we will use two sets of metrics one for the classification and one for the regression.

3.1.1 Classification

For evaluation of the classification, we will use F1 score and ROC curve in addition to Matthews correlation coefficient and recall-precision curve. We will compare the wet-dry classification with the radar reference taken along each CML as was described in the section 2.2.2.

Matthews correlation coefficient (MCC)

MCC is similar to F1 score, but F1 score takes into account only true positives(TP), false positives(FP), and false negatives(FN). Where MCC computes from all before and true negatives(TN). That is why it is more balanced and captures classification better for both classes. MCC is computed as

$$\mathrm{MCC} = \frac{\mathrm{TP} \cdot \mathrm{TN} - \mathrm{FP} \cdot \mathrm{FN}}{\sqrt{(\mathrm{TP}+\mathrm{FP})(\mathrm{TP}+\mathrm{FN})(\mathrm{TN}+\mathrm{FP})(\mathrm{TN}+\mathrm{FN})}} \tag{3.1}$$

Precision-recall curve

Similarly to the TPR-FPR(TPR - true positive rate, FPR - false positive rate) relationship in the ROC curve we can look at the precision-recall curve. The advantage of the precision-recall curve is that it is suitable for imbalanced datasets, and it tests classifier performance for both classes.

3.1.2 Regression

In the regression task, we will estimate rain intensity and for better comparison also the amount of rainfall for different aggregation times. We will use this to compare RMSE(root mean square error), MAE(mean absolute error), and NRMSE(normalized root mean square error), which we will compute as in [14]

$$\mathrm{NRMSE}(\hat{\boldsymbol{x}}, \boldsymbol{x}) = \frac{\sqrt{\frac{1}{N}\sum_i (x_i - \hat{x}_i)^2}}{\frac{1}{N}\sum_i x_i} \tag{3.2}$$

$\hat{\boldsymbol{x}}$ is estimated values and is $\boldsymbol{x}$ reference values.

We will compare the mean of the rain intensities in the rolling window of 15 minutes and for accumulated rainfall we will use aggregation times of one hour, six hours, 12, and 24 hours. Our reference is weather radar rain intensity taken along the path of each CML.

3.2 Weather radar comparison with rain gauges

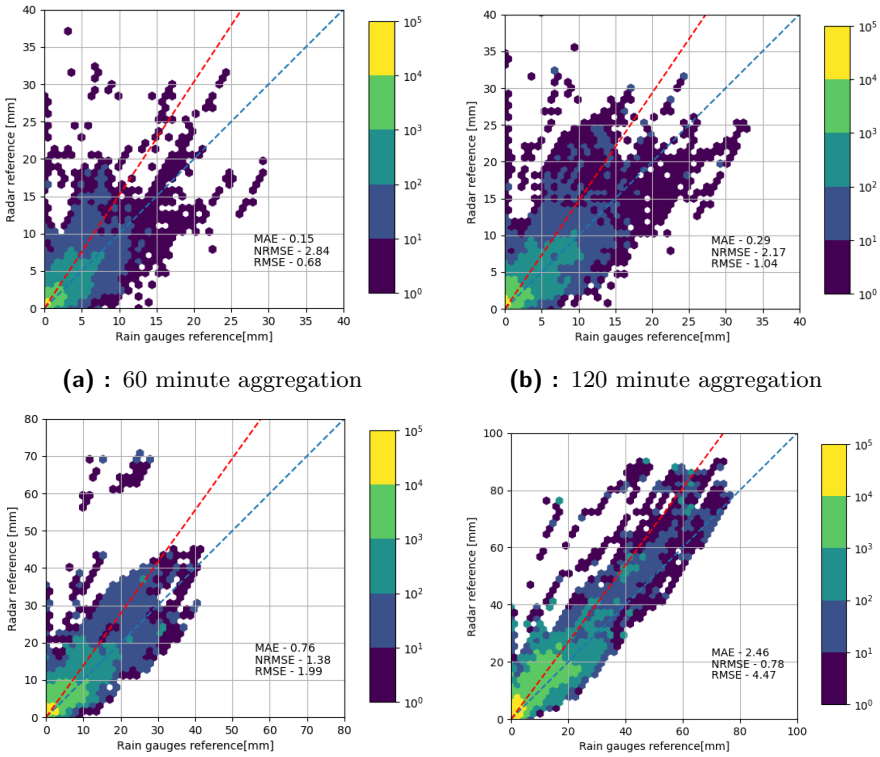

(a) : 60 minute aggregation **(b) :** 120 minute aggregation

(c) : 6 hour aggregation **(d) :** 24 hour aggregation

Figure 3.1: Comparison of weather radar with the rain gauges for time intervals from 1 hour to 24 hours. The blue dashed line is an ideal relationship between measured rainfalls and the red dashed line is a linear fit using the least squares method

Before comparison of the different methods for the rainfall estimation and the wet-dry classification, we will compare weather radar with the rain gauges, to better understand the limitations of using weather radar as our reference.

We start with the comparison of the rain gauges with direct measurements taken from the radar pixels on locations where the rain gauges are placed, without considering a wider area. Scatter plots for the different time aggregations for all rain gauges during 2015 can be seen in the figure 3.1.

There is visible evidence of the correlation between weather radar and rain gauges, however it is not perfect, and especially for the higher rain intensities it differs. This difference can be observed especially during the summer season as we can see in the figure 3.2.

The reason why radar differs especially for the higher rain intensities is apart from that radar is an indirect measurement of the rainfall as was mentioned in the section 1.2.2. But also because our data from the radar

have a logarithmic scale, which means higher steps towards the higher rain intensities and therefore less accurate measurements, for example, there are five steps between 1 mm/h and 10 mm/h but only one step between 10 mm/h and 20 mm/h.

This difference is more visible on some rain gauges as can be seen in the figure 3.3.

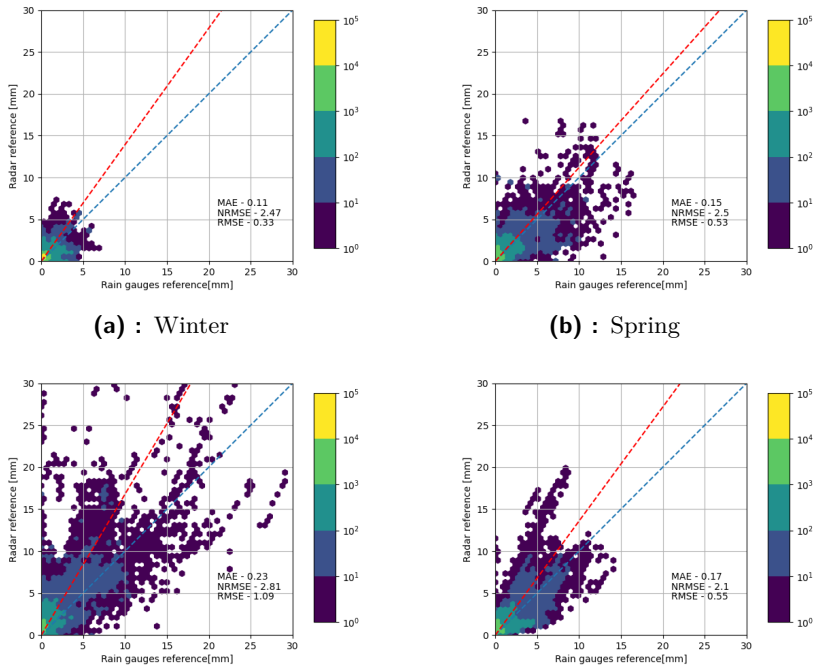

(a) : Winter **(b) :** Spring

(c) : Summer **(d) :** Autumn

Figure 3.2: Comparison of weather radar with the rain gauges for different seasons with one hour aggregation

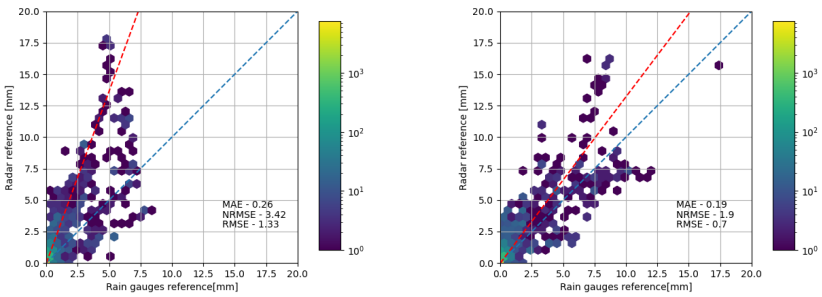

(a) : RG1 **(b) :** RG10

Figure 3.3: Comparison of the RG1 and RG10 rain gauges with the radar reference with one hour aggregation

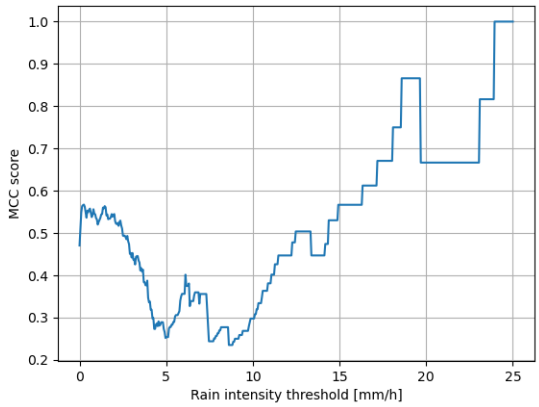

Figure 3.4: Wet-dry classification from weather radar using rain gauges as a reference with time aggregation of 15 minutes and without spatial aggregation. Flat parts of the graph are caused by the logarithmic scale of the radar.

Additionally, we plotted the wet-dry classification MCC score of weather radar to the rain gauges, where we can see in the figure 3.4 that for wet-dry classification from weather radar, it is best to select either low threshold or high threshold.

3.2.1 Spacial correlation of weather radar with rain gauges

In the second step, we considered a 1 km to 5 km radius area around each rain gauge. The difference between taking weather radar measurements directly in the location of the rain gauges and considering the wider area around them does not appear to be substantial compared to the effect of the time aggregation. In the figure 3.5 we compare the effect of both time and spacial aggregation.

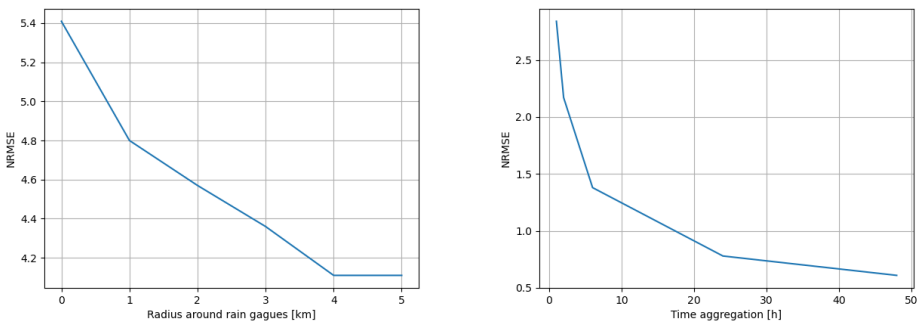

(a) : Relationship between NRMSE and spacial aggregation

(b) : Relationship between NRMSE and time aggregation

Figure 3.5: Effect of time and spacial aggregation on NRMSE error between the rain gauges and weather radar

3.3 Wet-dry classification

We evaluated three different network architectures and compared them with two other methods that are used for the wet-dry classification as we described at the beginning of this chapter.

Initially, we started with an evaluation on a few selected links to see how well each method performs and to see how different link parameters, especially length and frequency, affect performance, later on, we selected the best-performing architecture and extended it for usage with multiple links. We also created simulated data for one CML (link 444), parameters of selected links are in the table 3.1.

Optimization of hyperparameters for all methods was done on part of the train set with MCC selected as the criteria function. The selection of the parameters was done using a grid search. For the RSD method and the neural networks coefficients were set for each link individually. We compared both MCC and F1 scores. In this section, we used the "individual" dataset for the training and the evaluation.

Link ID	length [m]	frequency[GHz]	polarization
56	3195	25.56	V
63	2611	31.82	V
253	2546	24.55	H
444	854	35.63	H

Table 3.1: Selected link parameters

Method/Link ID	56	63	444	253	sim
RSD	0.42	0.43	0.35	0.37	0.34
Threshold	0.48	0.26	0.21	**0.48**	0.05
ResNet	0.52	0.39	0.32	0.43	0.70
Recurrent	0.46	0.39	0.34	0.43	0.68
Novota	**0.54**	**0.46**	**0.41**	0.44	**0.74**

Table 3.2: F1 score, sim are simulated data for link 444

Best performing network for the wet-dry classification is the network proposed by P. Novota in [13]. Second best performing networks are ResNet and the recurrent network. Simple thresholding works well on links where baseline does not change too much however when baseline changes as in the case of links 63 and 444 and simulated link it suffers big performance loss. All neural networks performed comparably better on the simulated link than other methods.

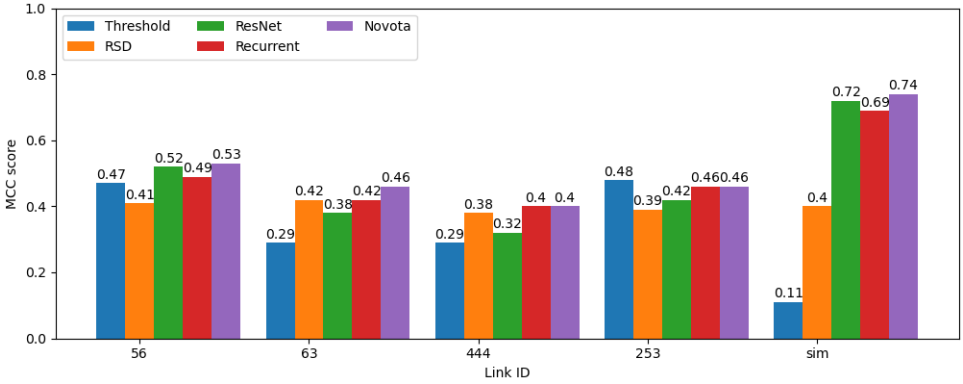

Figure 3.6: MCC score comparison

When we will look at the confusion matrices of each method for example for the link 444 in the figures 3.7 and 3.8. We see that the recurrent network performs better for rain detection (not wet-dry classification) than other methods, which corresponds with higher TPR(true positive rate) and lower FNR(false negative rate). The reason why F1 score and MCC score of the recurrent network and other methods are similar despite the difference between their FPR and TPR is that the recurrent network also has slightly worse FPR(false positive rate)but only about 2%, but because unbalanced test set consist around from 95% of dry samples it makes a big difference for the absolute value of the false positive samples.

This ratio of dry to wet samples is even higher for higher thresholds. For example for the threshold of 5 mm/h wet periods make only around 2% of our test set. For this reason, we will evaluate performance for different intensities using TPR also called recall score, which tells us the probability that the network will catch the rainy period if the rain intensity is higher than some predefined threshold. To have comparable results we set hyperparameters for each method so that the number of the false positive samples is the same across all methods.

This comparison for different rain intensities is shown in the figures 3.9, 3.10.

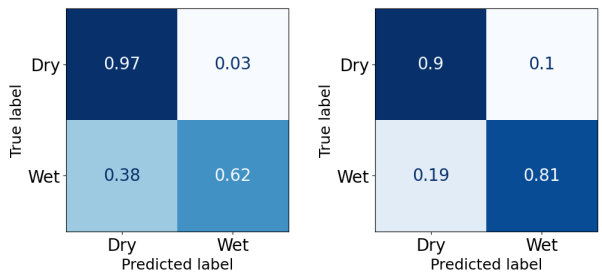

(a) : RSD **(b) :** Threshold

Figure 3.7: Confusion matrices for different methods for the link 444. All methods have hyperparameters set to maximize MCC score on the part of the train set as was described in the beginning of this section

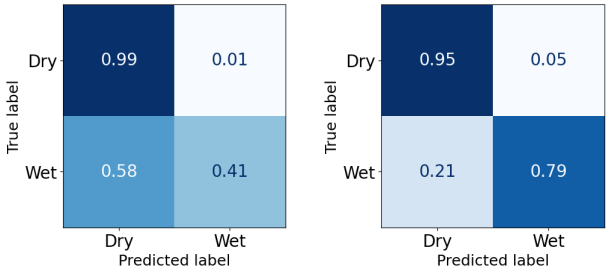

(a) : Novota **(b) :** Recurrent

Figure 3.8: Confusion matrices for different methods for the link 444

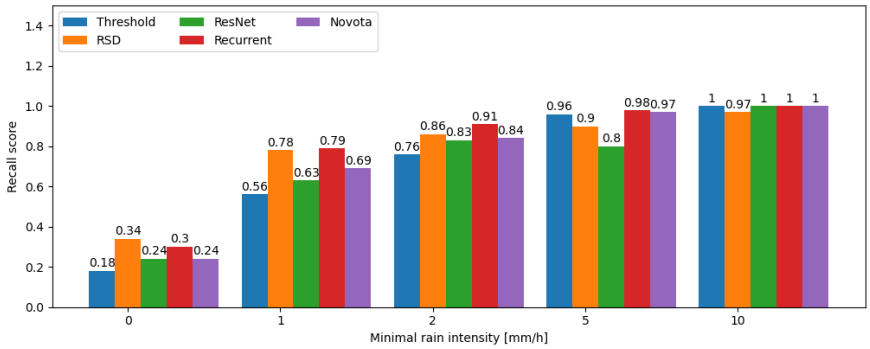

Figure 3.9: Recall score for different minimal rain intensities for link 444

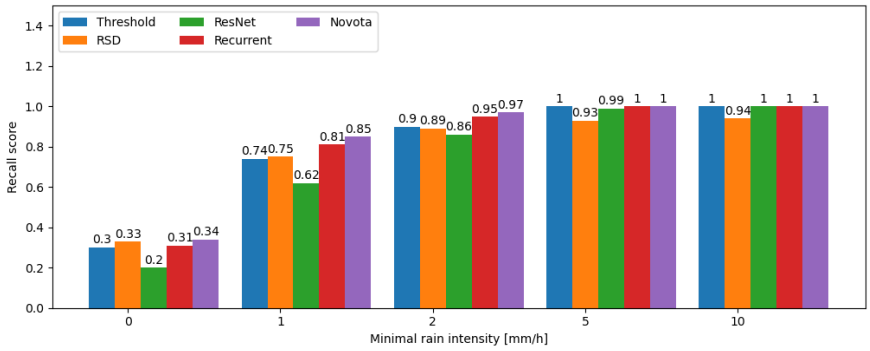

Figure 3.10: Recall score for different minimal rain intensities for the link 253

The difference between classification performance for the methods can be also visualized using a precision-recall curve and ROC curve. In the figure 3.11 are ROC and precision-recall curves for the link 253.

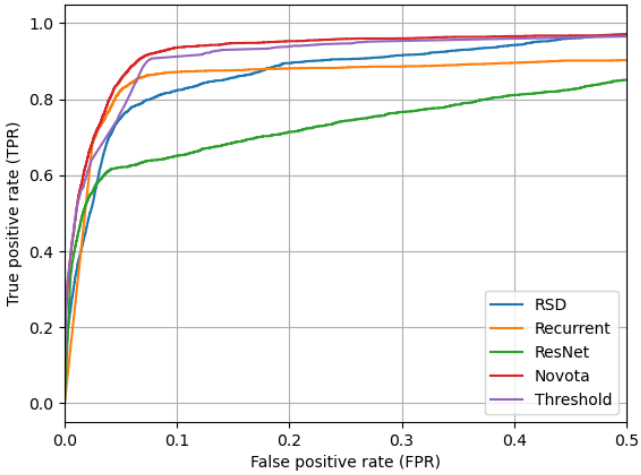

(a) : ROC curves

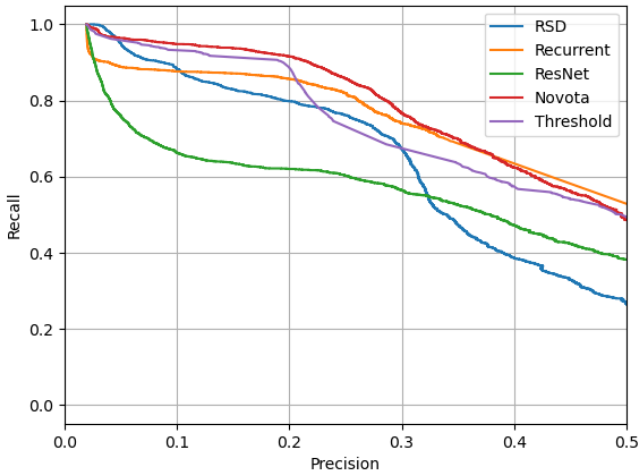

(b) : Precision-Recall curves.

Figure 3.11: ROC and Precision-Recall curves for link 253

An example of the wet-dry classification for two selected methods (RSD and the recurrent network) can be seen in the figure 3.12. It is noticeable that the recurrent network has less number of missed wet periods but a larger number of falsely detected wet periods, however if we take a closer look we can see that in these periods is raining but below our selected threshold of 1 mm/h.

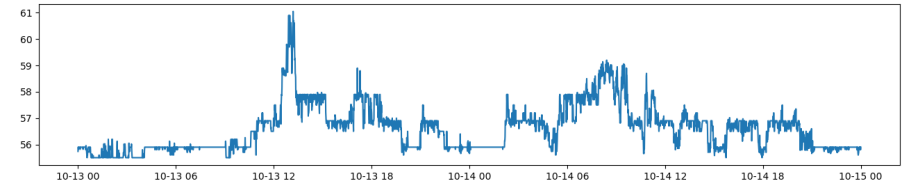

(a) : Link attenuation

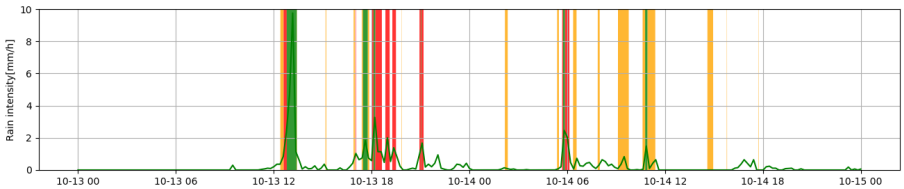

(b) : Classification based on RSD

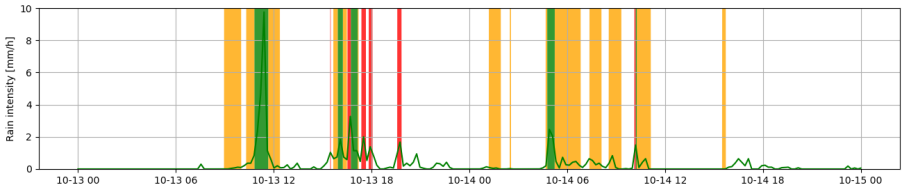

(c) : Classification based on recurrent network

Figure 3.12: Examples of the wet-dry classification for link 253, green is correctly classified wet period, orange is falsely detected wet period and red is missed wet period

3.4 Rainfall estimation

For the rainfall estimation, we compared the model-based method with two different baseline estimations described in the chapter 1.1. We compared it together with three of our methods and the neural network by P. Novota. The table 3.3 with the resulting RMSE comparison to weather radar reference is shown below.

To use the model-based method we needed to set WAA model coefficients. We have done this by selecting $d = 0.1$ as was also selected in [6] and then performing a grid search for the remaining two parameters C, z. We set WAA model coefficients individually for each CML. Selection of the coefficients was based on minimizing RMSE for rain intensities over 1 mm/h on part of the training set. The scatter plot of WAA parameters is in the figure 3.13. For the dynamic baseline method, we needed to select a function that would estimate the baseline, we selected the median because it has the best results. In this section, we used the "individual" dataset for the training and the evaluation.

Results show that the recurrent network has comparable results with other methods. The only exception is for the link 444 where we can see a big difference between the model-based method and neural networks. When we take a closer look at the outputs of each method in the figure 3.14, we will understand why.

Method/Link ID	56	63	444	253	sim
Static	**0.48**	0.74	2.75	0.40	0.74
Dynamic	0.50	0.46	2.75	0.41	0.43
ResNet	0.55	0.54	0.58	0.46	0.49
Recurrent	0.49	0.55	**0.54**	**0.39**	0.30
WAA	0.51	**0.45**	0.99	**0.39**	0.51
Novota	0.49	0.85	0.65	0.41	**0.21**

Table 3.3: RMSE values for different methods

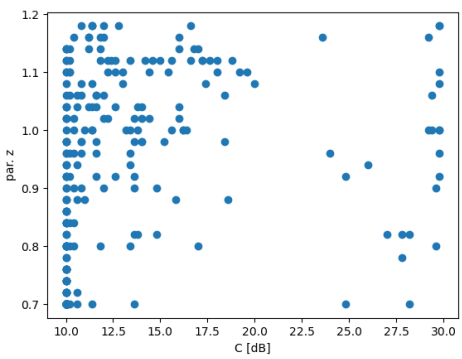

Figure 3.13: Distribution of WAA coefficients for model-based estimation method

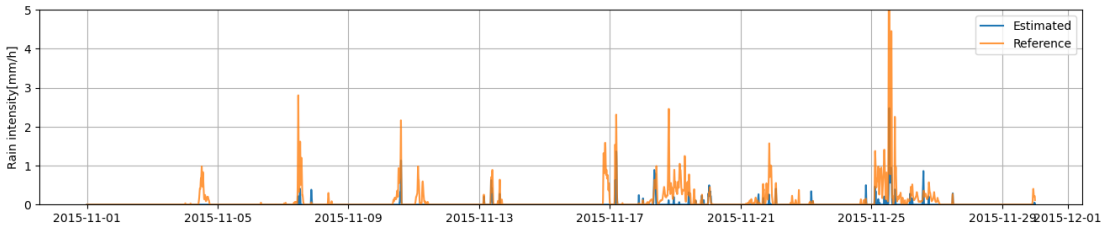

(a) : Static baseline method with optimal WAA coefficients sets using grid search

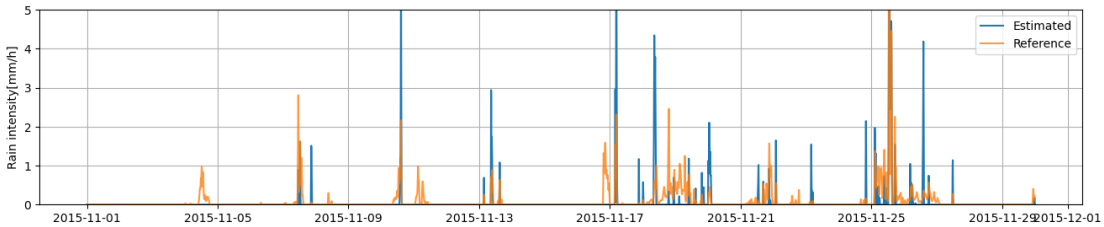

(b) : Static baseline method with lower WAA coefficients compared to figure (a)

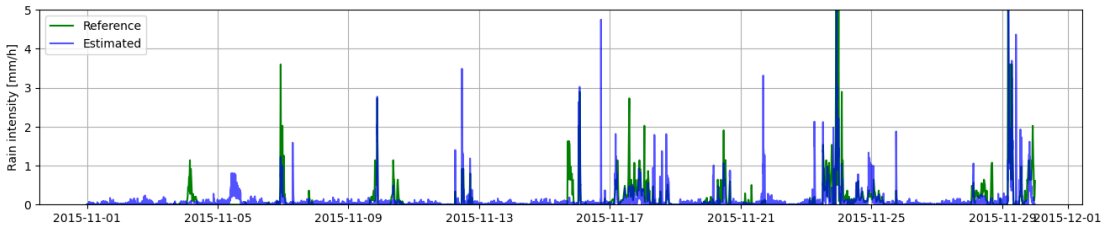

(c) : Recurrent network

Figure 3.14: Rain intensity estimation on link 444 for different methods

WAA correction for this link is so high that it suppresses the light rain, but with lower WAA correction it overestimates larger rain intensities and thus the RMSE is even higher.

This suggests that the link probably has atypical WAA or baseline behavior instead of being faulty, otherwise, there would not be improvement with the usage of neural networks.

We also compare RMSE for different rain intensities for the links 63 and 253.

Method/Rain intensity[mm/h]	0-1	1-5	5-15	15-25	25+
Static	**0.11**	1.76	5.63	**6.93**	**2.19**
Dynamic	**0.11**	1.94	6.22	9.33	3.81
ResNet	0.12	1.79	5.99	15.9	25.33
Recurrent	0.12	**1.43**	**5.02**	14.53	27.76
WAA	0.12	1.44	5.2	16.9	18.99
Novota	**0.11**	1.57	5.56	15.24	22.07

Table 3.4: RMSE values for different rain intensities for link 253

Method/Rain intensity[mm/h]	0-1	1-5	5-15	15-25	25+
Static	0.59	1.88	5.09	18.2	29.32
Dynamic	**0.11**	2.03	5.8	19.25	30.10
ResNet	0.28	1.75	5.25	13.52	30.77
Recurrent	0.55	**1.44**	**4.33**	18.39	29.24
WAA	0.19	1.48	4.5	18.08	**28.4**
Novota	0.75	1.56	4.78	**17.96**	29.24

Table 3.5: RMSE values for different rain intensities for the link 63

And comparison with NRMSE for selected methods is shown in the figures 3.15 and 3.16.

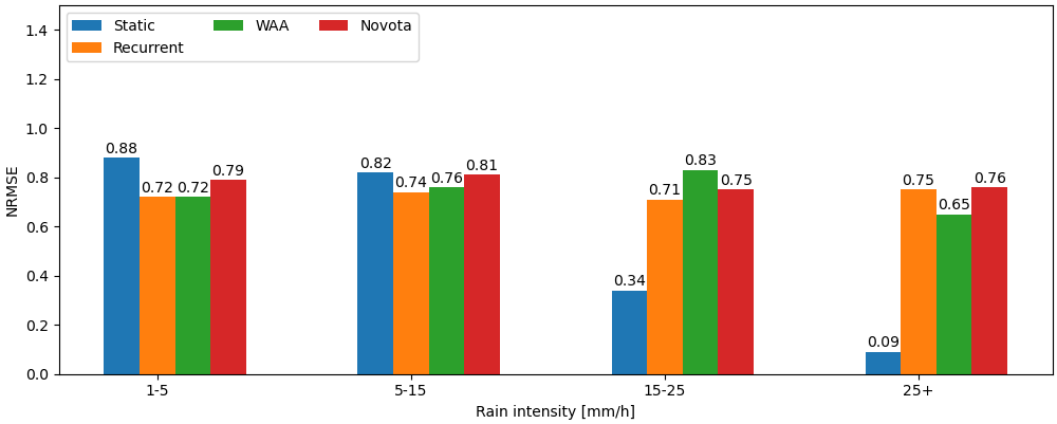

Figure 3.15: NRMSE of selected methods for different rain intensities for link 253

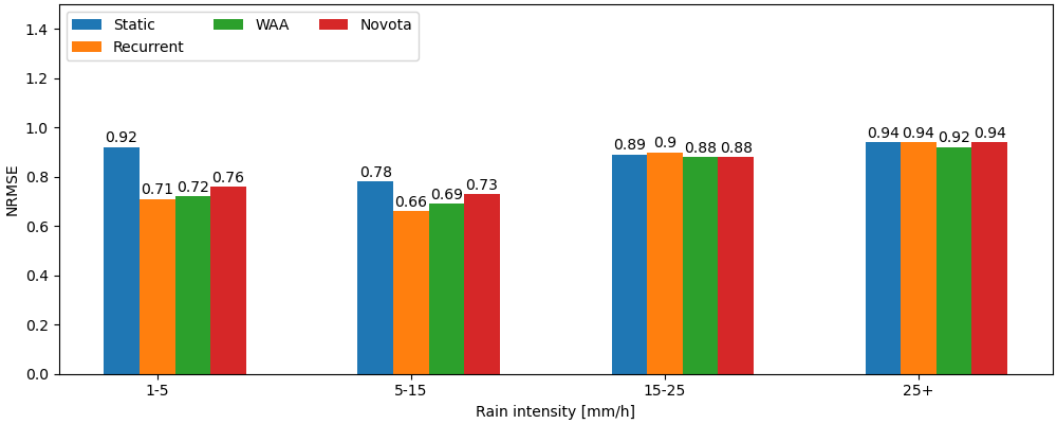

Figure 3.16: NRMSE of selected methods for different rain intensities for the link 63

We omitted rain intensities between 0-1 mm/h because they are too small and NRMSE error is too high for them even with little error, and therefore differences for other rain intensities would not be that visible, due to the scaling of the plot.

The recurrent network performs better for lighter rain and tends to underestimate higher rain intensities, this is probably because the distribution of the higher rain intensities in our dataset is lower compared to the lower rain intensities see figure 2.4, and thus neural network does not have enough samples to learn from. The opposite situation is for standard methods, where they tend to underestimate lower rain intensities.

This is more visible when we compare scatter plots for different time aggregations.

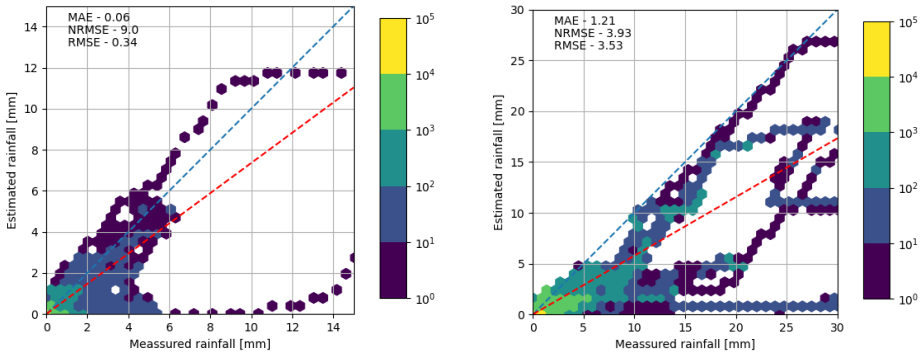

(a) : 1 hour aggregation **(b) :** 24 hours aggregation

Figure 3.17: Static baseline method

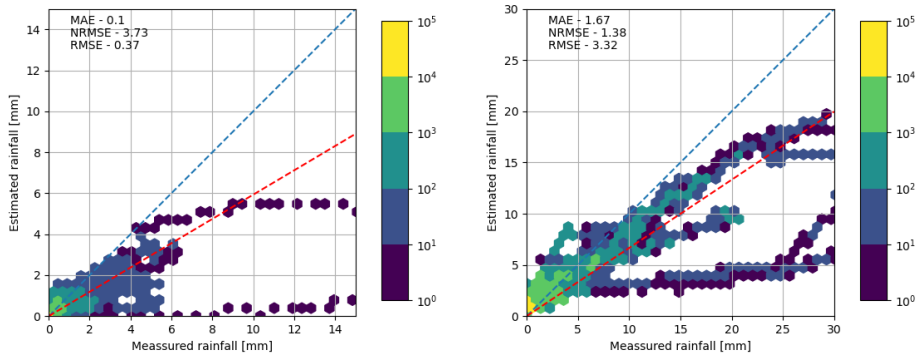

(a) : 1 hour aggregation **(b) :** 24 hours aggregation

Figure 3.18: Recurrent network

3.5 Multi-link rain estimation

In the previous two sections, we compared the performance of our methods on the group of selected links. Based on the results we selected the recurrent model as the best-performed one and extended it to support multi-link learning as was described in section 2.5.3. We trained the recurrent network(recurrent) and compared it with static baseline method(static), furthermore, we also used robust learning described in section 2.5.5 and compared the results(recurrent - robust). We will use in the all figures and tables names that are in the brackets behind each method. Furthermore, we performed cross-validation by dividing the dataset into five smaller sets. With cross-validation, we also have the advantage, that we can use all links for both training and testing. In this section, we used the "multi" dataset for the training and the evaluation.

3.5.1 Link-based comparison

Initially, we estimated rainfall predictions for every link and compared it with its weather radar reference along its path as was described in 2.2.2, resulting scatter plots for different time aggregations are shown in the figures 3.19, 3.20, 3.21 and 3.22.

RMSE and NRMSE are lower for the recurrent network. The recurrent network is especially better at estimating lower rain intensities see table 3.7, however as we can see it tends to underestimate higher rain intensities. One of the reasons why the recurrent network is better is because it can filter out spikes in signal attenuation. These spikes are caused by the jumps in the signal attenuation during strong rainfall events, but often happen also during dry periods, they are causing high overestimations in the rain intensity for model-based methods. In the picture 3.23, we compare the static baseline method and the recurrent network. These spikes are also the reason why we have such a high RMSE for static baseline method for intensities between 0 and 1.

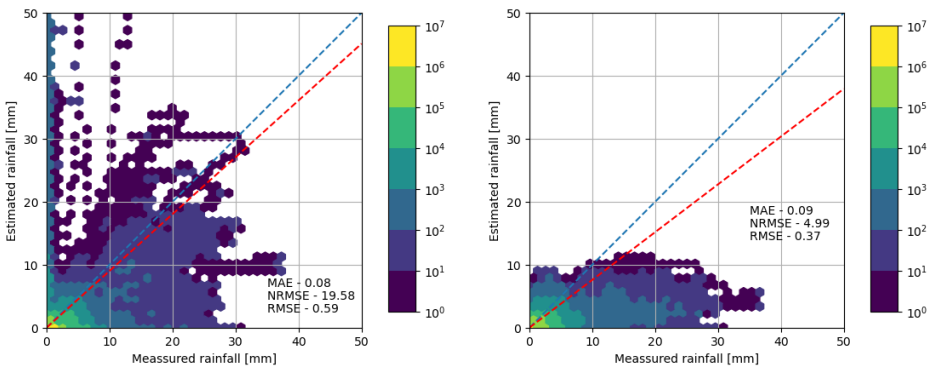

(a) : Static baseline method

(b) : Recurrent network

Figure 3.19: Comparison of CML estimated rainfall with radar reference for one hour aggregation

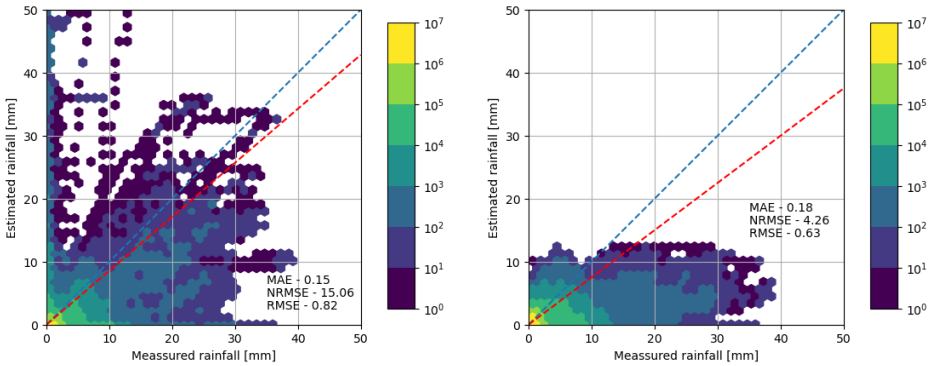

(a) : Static baseline method **(b) :** Recurrent network

Figure 3.20: Comparison of CML estimated rainfall with radar reference for two hour aggregation

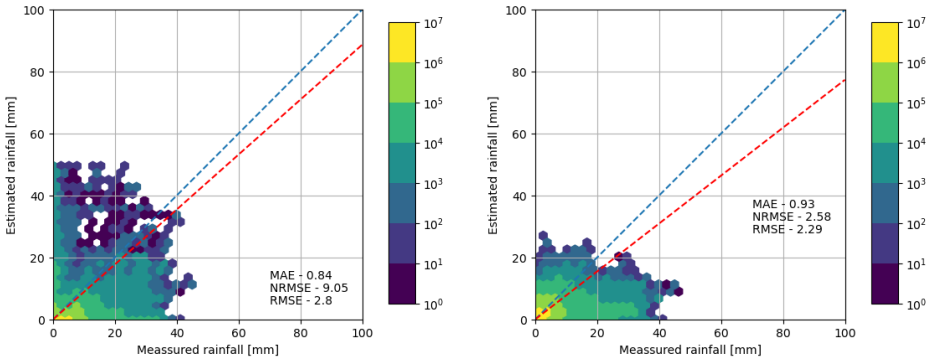

(a) : Static baseline method **(b) :** Recurrent network

Figure 3.21: Comparison of CML estimated rainfall with radar reference for twelve hour aggregation

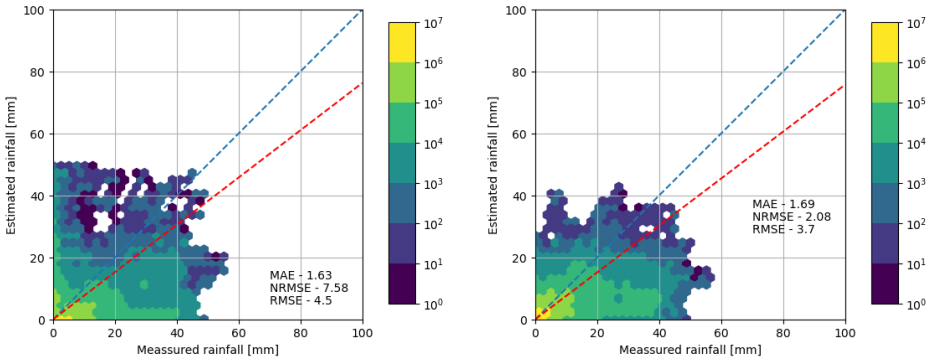

(a) : Static baseline method **(b) :** Recurrent network

Figure 3.22: Comparison of CML estimated rainfall with radar reference for 24 hour aggregation

Method/Time aggregation[h]	1	2	6	12	24
Static	0.59	0.82	1.71	2.8	4.5
Recurrent	**0.37**	**0.63**	**1.41**	**2.29**	**3.70**
Recurrent - robust	0.40	0.70	1.64	2.81	4.83
Graf et al.	0.42	-	-	-	4.16

Table 3.6: RMSE comparison with radar reference for different time aggregations.

Method/Rain intensity[mm/h]	0-1	1-5	5-15	15-25	25+	all
Static	16.31	2.15	9.11	16.94	**27.43**	16.17
Recurrent	**0.15**	1.81	5.74	16.03	34.28	**0.45**
Recurrent - robust	0.22	**1.8**	**5.72**	**16.02**	34.33	0.48
Habi et al.	-	-	-	-	-	(0.31|0.43)
Graf et al.	-	-	-	-	-	0.52

Table 3.7: RMSE values for different rain intensities using all CML links.

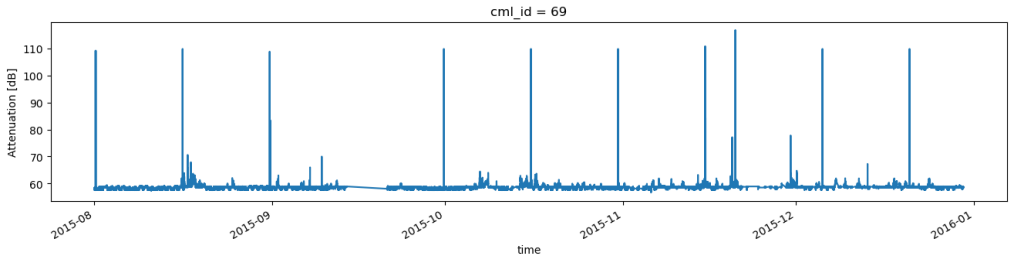

(a) : Link attenuation

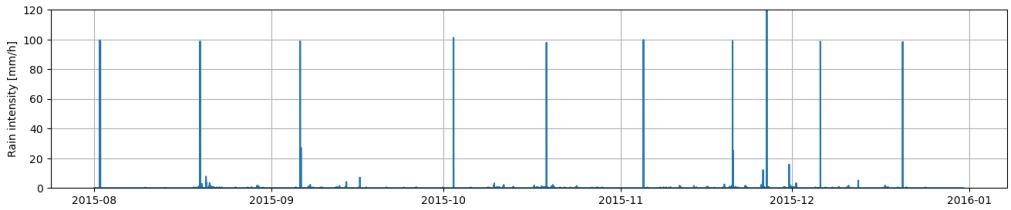

(b) : Static baseline method rain intensity estimation

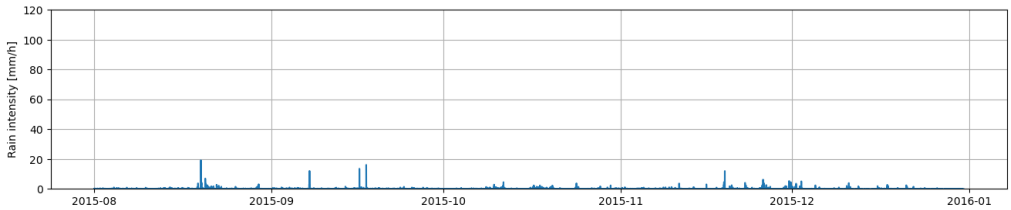

(c) : Recurrent network rain intensity estimation

Figure 3.23: Spikes in attenuation of the link 69

From comparison in the table 3.7 we do not see a big difference between the recurrent network trained with and without the usage of robust learning, this could be because as we had shown network itself is good at learning to filter unreliable data even without the usage of robust learning. The performance of the recurrent network was better for all rain intensities except 25+ mm/h than for the static baseline method.

In the table 3.6 we also compared results from Graf et al. [8]. Where they evaluated using the static baseline method (with different settings than ours) data of 3904 CMLs in Germany during one year. We took RMSE values for hourly and daily aggregated data from their figure 6 for September, October, and November in their figure referred to as "SON", because our test set spans from August to December.

In the table 3.7 we compared with Habi et al. network [14]. Their results are taken from the table IV for the TSN method, the first number is for the Israel region and the second is for the Sweden region. Values for Graf et al. were taken from their table 2 as a mean of RMSE in the row with criteria none for August to December.

3.5.2 Map-based comparison

To better compare the spatial correlation of rainfall predictions on multiple CMLs with weather radar reference we need to interpolate CML rainfall estimations in space, as an interpolation method we used inverse distance weighting described in chapter 2.5.6. The output grid resolution of IDW is the same as the weather radar. In the table 3.8 we compare the performance of the recurrent network, static baseline method, and interpolation from rain gauges.

Method/Aggregation time	1h	2h	6h	12h	24h
Static	1.71	1.65	6.77	10.54	16.73
Recurrent	0.33	**0.54**	**1.09**	**1.63**	**2.52**
Recurrent - robust	0.40	0.57	1.36	2.25	3.8
Rain gauges	**0.29**	0.55	1.4	2.30	3.85

Table 3.8: RMSE between methods and radar maps with different time aggregations

For one map the MSE is

$$\mathrm{MSE}(\hat{\boldsymbol{x}}, \boldsymbol{x}) = \frac{1}{N_x N_y} \sum_{x=0}^{N_x} \sum_{y=0}^{N_y} (\hat{x}_{xy} - x_{xy})^2 \tag{3.3}$$

N_x, N_y are a number of pixels in the grid, $\hat{\boldsymbol{x}}$ are estimated values $\boldsymbol{x}$ are true values. For multiple maps, we compute RMSE as the mean of MSE for each

snapshot

$$\mathrm{RMSE}(\hat{\boldsymbol{x}}, \boldsymbol{x}) = \sqrt{\frac{1}{N}\sum_{i=0}^{N}\mathrm{MSE}(\hat{x}_i, x_i)} \tag{3.4}$$

N is a number of snapshots.

An example of interpolation maps is shown in the figures in appendix A.

We can observe that except for one hour aggregation the recurrent method was in map-based comparison better than other methods and better than rain gauges, which is not surprising because there are only 23 rain gauges vs 422 CML links.

Chapter 4

Discussion

In this work we investigated the usage of the weather radar as a reference for the wet-dry classification and the rainfall estimation from the commercial microwave links, we also compared methods based on the models for the link attenuation with our methods based on deep learning. We initially started with a comparison on selected group of links each one trained individually, and then we extended best performing network architecture for the rainfall estimation on all links and tested the filtration of the outliers using robust learning.

In the chapter about wet-dry classification 3.3 we concluded that the network of P. Novota had better performance than other methods, however for all methods, F1 scores and MCC scores were quite low. This could be because of our selected threshold of 1 mm/h, because as we saw in the figure 3.4 the best possible MCC score for the 1 mm/h threshold is around 0.6 when using weather radar as our reference. Another cause as we saw in the chapter 3.2 is that weather radar is not as accurate as the rain gauges and sometimes can detect water droplets in the atmosphere that do not drop to the ground.

For the rainfall estimation task, the recurrent network had better results than other methods for the rain intensities between 1 and 15 mm/h. The recurrent network had better RMSE for all rain intensities as shown in the table 3.3 only for the links 253 and 444. Link 444 was particularly challenging as can be seen in the picture 2.1, it is short so WAA is bigger proportionally to rain-induced attenuation and also has sudden changes in the signal attenuation, which as we mentioned is problematic for model-based method without proper filtration. The ResNet model did not perform very well, this could be caused by batch normalization within the network that normalizes the data, and therefore it, is harder for the network to train for regression, but without it ResNet was problematic to train. ResNet is also complex a network with many hyperparameters, and adjusting them right is not an easy task, therefore with different hyperparameters and settings ResNet could achieve better results.

The last step was an extension of the best-performed neural network architecture for rainfall prediction, in our case the recurrent network, to support learning from multiple links. For this task, we saw the biggest improvement in comparison. The improvement was not only in terms of RMSE or NRMSE

but moreover it had lower dispersion of values, especially for one and two hour aggregations as can be seen in the figures 3.19 and 3.20, however, on the other hand, it tended to underestimate higher rain intensities. From the table 3.7, we found that using robust learning gave slightly better results, but when we interpolated values in space and compared them with radar snapshots the recurrent network without robust learning performed better. The cause of this behavior could be because the recurrent network itself is good at filtering unreliable data and therefore usage of robust learning did not make a big difference. Another reason why robust learning performed worse in comparison to interpolated data could be because excluded links during training contained useful information, or they were not faulty.

In link-based comparison with the recurrent network of Habi et al., [14], we had worse performance compared to their results. On the other hand, we had better results than Graf et al. [12] as was shown in the table 3.6, however their dataset was larger than ours (3904 CMLs).

Chapter 5

Conclusion

In this work, we investigated the usage of the weather radar reference for the wet-dry classification and the rainfall estimation from the perspective of evaluation on the group of individual links to evaluating on all available links. Additionally, we compared results with model-based methods in time and space.

We found that for wet-dry classification performed best the network from P.Novota [13] and for the rainfall estimation the recurrent network for rain intensities between 1 and 15 mm/h, was also better in the case of link-based comparison in the section 3.5.1 for rain intensities between 1 and 25 mm/h. We had better results than Graf et al. [12] but also worse than Habi et al. [14].

Similarly, we showed that weather radar as the reference can be used, however better results would be achieved with radar data with smaller quantization. Furthermore, we also created a method for generating synthetic data which can be used for further testing and evaluation of different methods.

Bibliography

[1] V. Christofilakis, G. Tatsis, *et al.*, "Earth-to-earth microwave rain attenuation measurements: A survey on the recent literature", *Symmetry*, vol. 12, 2020.

[2] H. Messer, A. Zinevich, *et al.*, "Environmental monitoring by wireless communication networks", *Science*, vol. 312, pp. 173–713, 2006.

[3] A. Overeem, H. Leijnse, *et al.*, "Retrieval algorithm for rainfall mapping from microwave links in a cellular communication networ", *Atmos. Meas. Tech.*, vol. 9, pp. 2425–2444, 2016.

[4] C. Chwala and H. Kunstmann, "Commercial microwave link networks for rainfall observation: Assessment of the current status and future challenges", *WIREs Water*, vol. 6, 2 2019.

[5] Schleiss, R. M., *et al.*, "Quantification and modeling of wet-antenna attenuation for commercial microwave link", *IEEE Geoscience and Remote Sensing Letters*, vol. 10, pp. 1195–1199, 2013.

[6] J. Pastorek, M. Fencl, *et al.*, "Precipitation estimates from commercial microwave links: Practical approaches to wet-antenna correction", *IEEE Geoscience and Remote Sensing Letters*, vol. 60, pp. 1–9, 2021.

[7] P. Valtr, M. Fencl, *et al.*, "Excess attenuation caused by antenna wetting of terrestrial microwave links at 32 ghz", *IEEE Antennas and Wireless Propagation Letters*, vol. 18, no. 8, pp. 1636–1640, 2019.

[8] M. Graf, C. Chwala, *et al.*, "Rainfall estimation from a german-wide commercial microwave link network: Optimized processing and validation for 1 year of data", *Hydrology and Earth System Sciences*, vol. 24, no. 6, pp. 2931–2950, 2020.

[9] M. Fencl, M. Dohnal, *et al.*, "Gauge-adjusted rainfall estimates from commercial microwave links", *Hydrology and Earth System Sciences*, vol. 21, pp. 617–634, 1 2017.

[10] M. Djibo, C. Chwala, *et al.*, "High-resolution rainfall maps from commercial microwave links for a data-scarce region in west africa", *Journal of Hydrometeorology*, vol. 24, no. 10, pp. 1847–1861, 2023.

[11] M. F. Rios Gaona, A. Overeem, *et al.*, "Rainfall retrieval with commercial microwave links in são paulo, brazil", *Atmospheric Measurement Techniques*, vol. 11, no. 7, pp. 4465–4476, 2018.

[12] J. Polz, C. Chwala, *et al.*, "Rain event detection in commercial microwave link attenuation data using convolutional neural networks", *Atmos. Meas. Tech.*, vol. 13, pp. 3835–3681, 7 2020.

[13] P. Novota, "Rain intensity estimation from cml link data", bachelorthesis, Czech technical university in Prague, 2022.

[14] H. V. Habi and H. Messer, "Recurrent neural network for rain estimation using commercial microwave links", *IEEE Transactions on Geoscience and Remote Sensing*, vol. 59, pp. 3672–3681, 5 2021.

[15] D. A. Segovia-Cardozo, C. Bernal-Basurco, *et al.*, "Tipping bucket rain gauges in hydrological research: Summary on measurement uncertainties, calibration, and error reduction strategies", *Sensors*, vol. 23, no. 12, p. 5385, 2023.

[16] Z. Sokol, J. Szturc, *et al.*, "The role of weather radar in rainfall estimation and its application in meteorological and hydrological modelling—a review", *Remote Sensing*, vol. 13, no. 3, 2021.

[17] (2010). Radarová síť czrad, [Online]. Available: `https://www.chmi.cz/files/portal/docs/meteo/rad/info_czrad/index.html` (visited on 05/10/2024).

[18] R. Uijlenhoet, "Raindrop size distributions and radar reflectivity–rain rate relationships for radar hydrology", *Hydrology and Earth System Sciences*, vol. 5, no. 4, pp. 615–627, 2001.

[19] I. Fawaz, H. Forestier, *et al.*, "Deep learning for time series classification: A review", *Data Mining and Knowledge Discovery*, vol. 33, pp. 917–963, 4 2019.

[20] T.-Y. Lin, P. Goyal, *et al.*, "Focal loss for dense object detection", *CoRR*, vol. abs/1708.02002, 2017.

[21] (2005). Specific attenuation model for rain for use in prediction methods (recommendation), [Online]. Available: `https://www.itu.int/dms_pubrec/itu-r/rec/p/R-REC-P.838-3-200503-I!!PDF-E.pdf` (visited on 05/18/2024).

[22] A. Rusiecki, *Trimmed Robust Loss Function for Training Deep Neural Networks with Label Noise*, L. Rutkowski, R. Scherer, *et al.*, Eds. Cham: Springer International Publishing, 2019, pp. 215–222, ISBN: 978-3-030-20912-4.

[23] H. V. Habi, "Rain detection and estimation using recurrent neural network and commercial microwave links", diplomathesis, Tel Aviv University, 2019.

[24] M. Fencl, P. Valtr, *et al.*, "Quantifying wet antenna attenuation in 38-ghz commercial microwave links of cellular backhaul", *IEEE Geoscience and Remote Sensing Letters*, vol. 16, no. 4, pp. 514–518, 2019.

[25] E. Kamtchoum, A. Nzeukou Takougang, *et al.*, "A machine learning approach for the classification of wet and dry periods using commercial microwave link data", *SN Computer Science*, vol. 3, 3 2022.

[26] N. Blettner, M. Fencl, *et al.*, "Transboundary rainfall estimation using commercial microwave links", *Earth and Space Science*, vol. 10, no. 8, 2023.

Appendix A

Interpolation maps

Below we include examples of the interpolation maps for the different rain intensities, where the methods are in the order of rows as static baseline, recurrent network, recurrent network with robust learning, rain gauges and radar reference. The time difference between each column is 15 minutes, without any space or time aggregation.

We will compare the interpolation maps for the low rain intensity (up to 5 mm/h), middle rain intensity (between 5 and 15 m/h) and high rain intensity (over 15 mm/h).

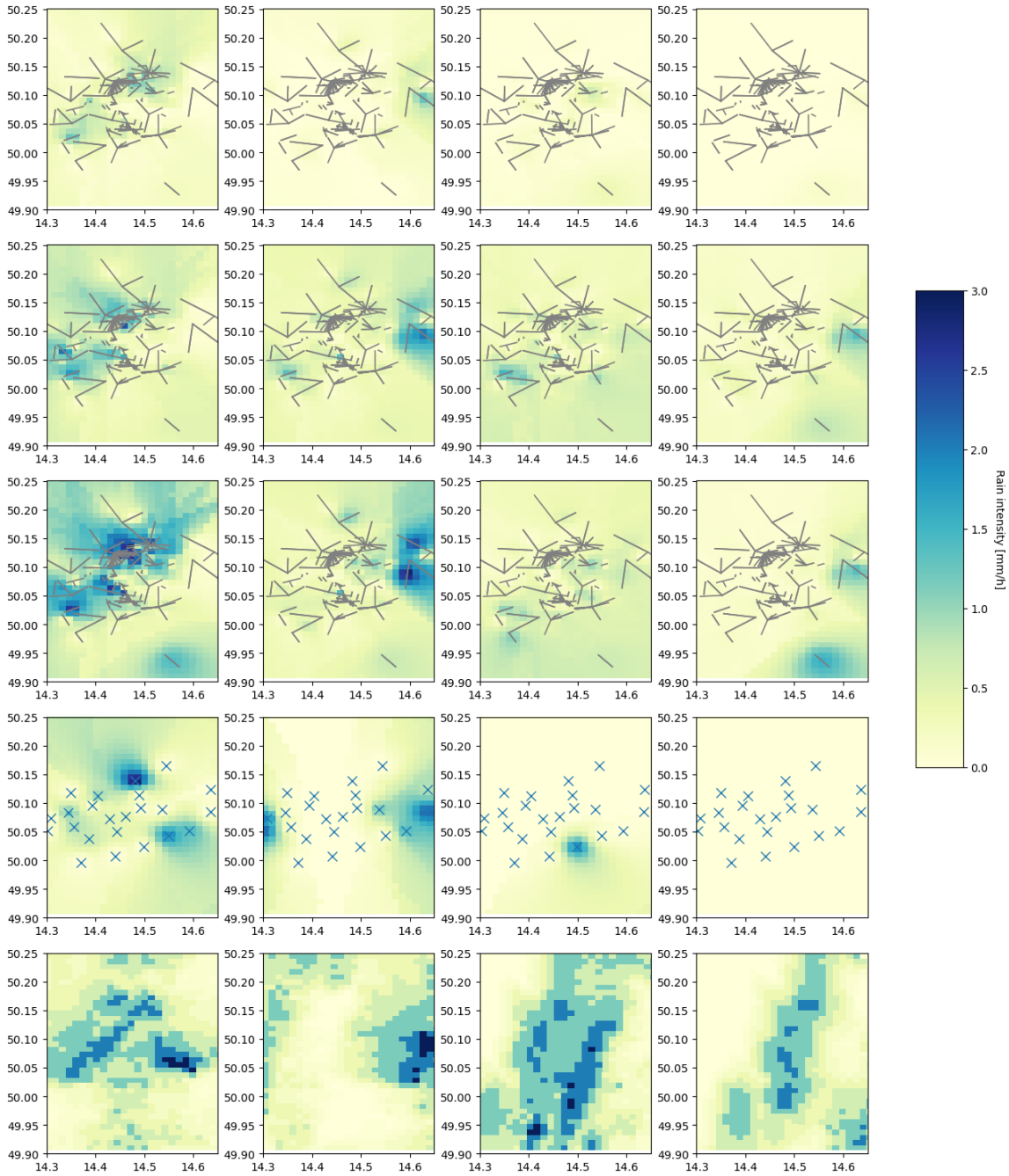

Figure A.1: Example of the interpolation maps for the different methods for the low rain intensity on 2015-08-16 14:00

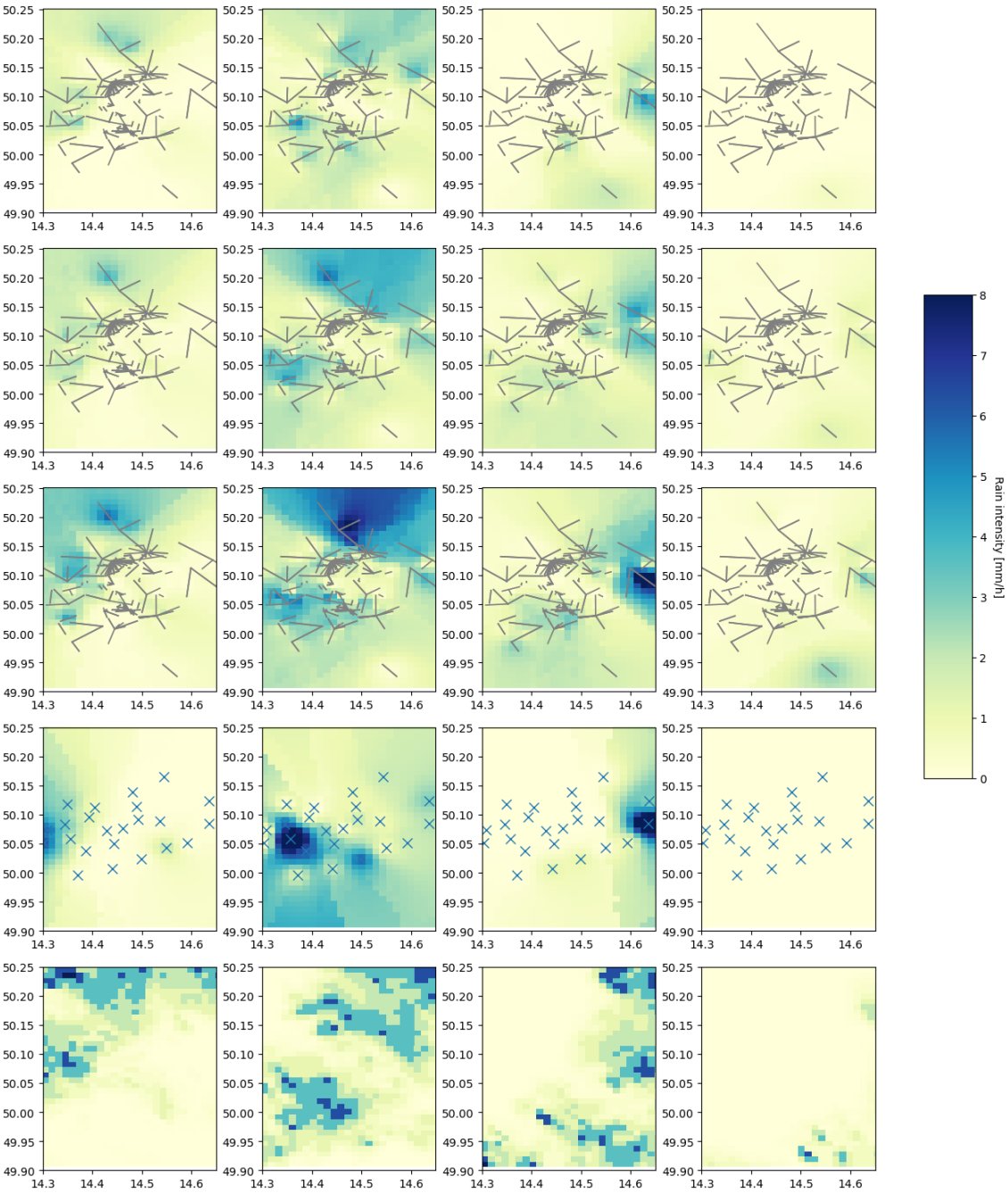

Figure A.2: Example of the interpolation maps for the different methods for the middle rain intensity on 2015-09-06 02:00

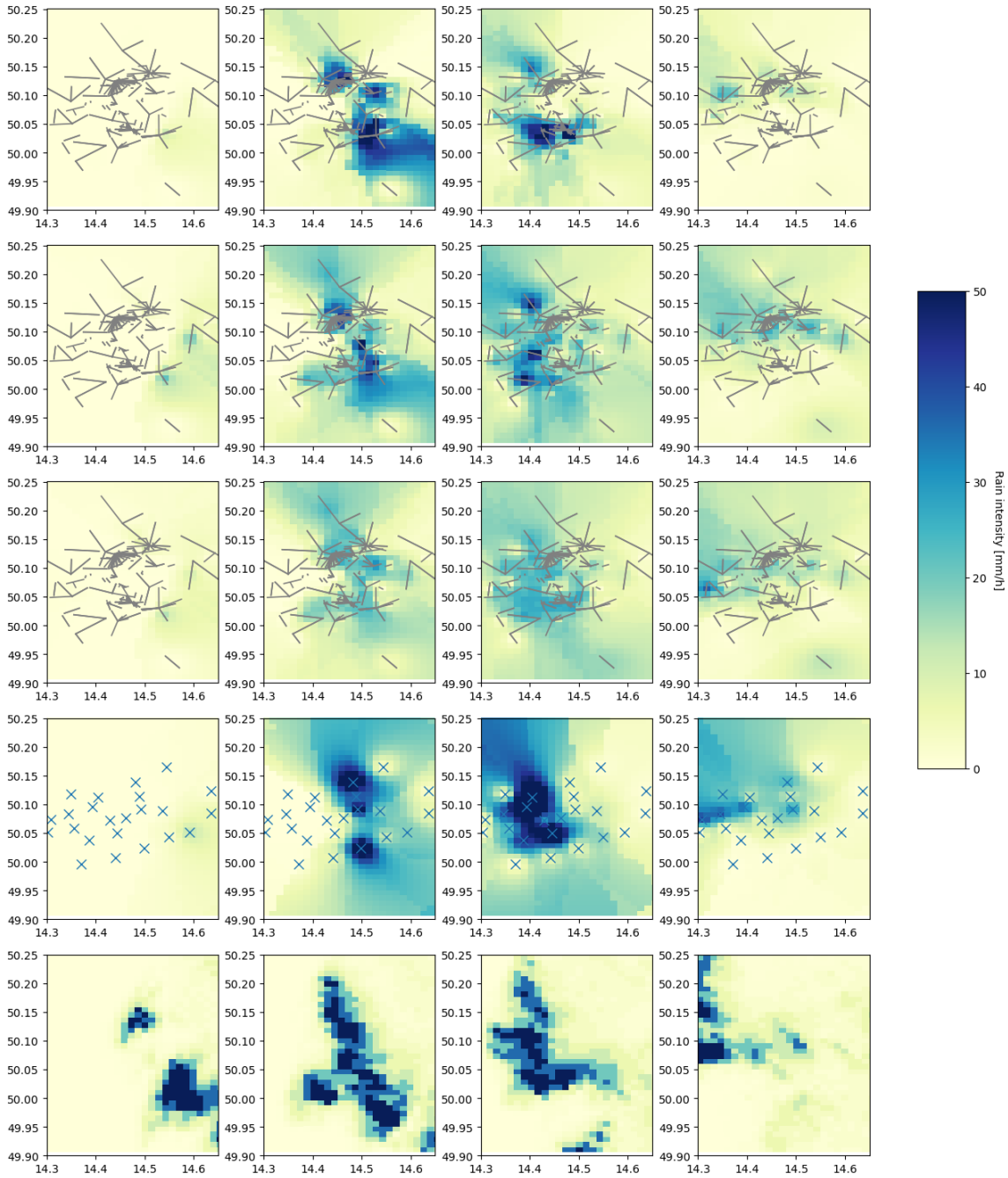

Figure A.3: Example of the interpolation maps for the different methods for the high rain intensity on 2015-09-07 12:30